

Challenges in identifying Antarctic coastal polynyas in satellite observations and climate model output to support ecological climate change research

Laura Landrum¹, Alice K. DuVivier¹, Marika M. Holland¹, Kristen Krumhardt¹, Zephyr Sylvester²

5 ¹NSF National Center for Atmospheric Research, Boulder, CO, USA

²INSTAAR, University of Colorado, Boulder, CO, USA

Correspondence to: Laura Landrum (landrum@ucar.edu)

Abstract. Antarctic coastal polynyas are key components of Antarctic marine ecosystems, influencing light and nutrient availability and open water access for marine predators. Thus, changes in the physical characteristics of polynyas can influence how these ecosystems respond to a changing climate. Here, we explore challenges inherent in identifying climatologically and biologically relevant Antarctic coastal polynyas on gridded data in both satellite and Earth System Model data. We find that it is critical to consider grid type and resolution, season, metric and threshold when defining polynyas. Regridding data, both spatially and temporally, can have significant impacts on identified polynya statistics. The spatial distributions of Antarctic coastal polynyas are significantly correlated between the two observational products as well as between the observational products and the model data. The Earth System Model we use here captures coastal polynya-like features that occupy ~3% of the area of the winter sea ice zone and contribute ~17-21% of the total sea ice zone marine net primary productivity (NPP). Temporal self- and cross correlations of integrated polynya areas and numbers are inconsistent across observational and modelling products. Trends in polynya areas are not robust, changing significance, magnitude and sign across threshold, grid and product.

20 **1 Introduction**

Polynyas, defined by the World Meteorological Organization as “any non-linear shaped opening enclosed in ice“ and “may contain brash ice and/or be covered with new ice, nilas, or young ice” (WMO, 1970), can be found in the southern ocean both in open water and along the Antarctic coast. Open water polynyas are created when relatively warm ocean water upwells to the surface thermodynamically melting sea ice (“sensible heat polynyas”) – these are relatively uncommon and will not be discussed further in this work. Coastal polynyas are driven by cold downslope winds off the Antarctic continent that mechanically push sea ice away from the coast leaving open ocean water that rapidly loses heat and freezes into more sea ice (“latent heat polynyas”). Many coastal polynyas, particularly in Eastern Antarctic, are associated with land fast ice and grounded icebergs which influence the location and size of the polynyas formed through blocking ice advection (e.g. Fraser et al., 2019; Nihashi & Ohshima, 2015). Coastal polynyas occupy only a small area within the Southern Hemisphere sea ice zone

30 yet play an outsized role in Antarctic sea ice production, deep water formation, global thermohaline circulation, carbon
sequestration, and biological activity. Coastal polynyas produce about 10% of the total Antarctic sea ice (Tamura et al., 2008)
and one polynya alone - the Cape Darnley polynya produces ~6-13% of the total Antarctic Bottom Water (Ohshima et al.,
2013). As regions of lower sea ice concentration and/or thinner sea ice, polynyas are the first oceanic regions within the sea
35 ice zone exposed to light in the Antarctic spring. As a result, polynyas show enhanced production within the Antarctic sea ice
zone, where phytoplankton growth tends to be limited by light (Arrigo and van Dijken, 2003; Arrigo et al., 2015) and spring
phytoplankton blooms within polynyas are frequently synchronized with light availability (e.g. Li et al., 2016). Polynyas also
provide Antarctic predators (e.g., penguins, seals) both open water access and augmented prey resources, with ephemeral
polynyas being of particular importance for Emperor penguins (Labrousse et al., 2019). Coastal polynyas are sometimes
referred to both as “polynyas“ (indicating formation in the ice-growth season) and “post-polynyas“ (formation in the melt
40 season by the rapid melting of the relatively thin sea ice), in recognition of their important biological functions even when they
may cease to be defined as “polynyas“ in the strict definition (e.g. Arrigo & van Dijken, 2003; Criscitiello et al., 2013).

How Antarctic marine ecosystems respond to a changing climate will be determined, at least in part, by changes in the sea
icescape, including the size, location and timing of coastal polynyas. Antarctic polynyas are formed within the sea ice zone,
45 and the sea ice around Antarctica has been studied extensively using both satellite and Earth system model (ESM) data. Satellite
observations of sea ice (1979-present) show small positive trends in Antarctic sea ice area (the total area of sea-ice) and extent
(defined as the area covered by sea ice concentrations of 15% or higher) until 2016 followed by unprecedented sea ice losses
accompanied by changes in both persistence and variability (e.g., Fogt et al., 2023; Parkinson 2019; Purrich & Doddridge,
2023; Raphael & Handcock, 2022; Raphael et al., 2025; Turner et al., 2017; Turner et al., 2022). The most current ESMs
50 contributing to the Climate Model Intercomparison Project phase 6 (CMIP6; Eyring et al., 2016) show a wide range of
Antarctic sea ice states (e.g. Roach et al., 2020). Even though many ESMs capture the climatology of observed Antarctic sea
ice, ESMs struggle to capture both the small, but significant, positive trend observed 1979-2015, and the more recent dramatic
sea ice losses (Diamond et al., 2024; Roach et al., 2020). The recent, extreme losses and extended reconstructions of Antarctic
sea ice suggest that there may be internal variability not captured by the relatively short observational record (e.g. Fogt et al.,
55 2023; Hobbs et al., 2024; Holmes et al., 2024; and references therein). These assessments of Antarctic sea ice, however, focus
predominantly on large-scale sea ice extent and area rather than the complex icescape within the ice pack where polynyas
form.

Polynyas and polynya-like features often have scales and dimensions much smaller than those resolved by either satellite
60 observations or global climate model data. For example, the median sizes of wintertime Antarctic coastal polynyas identified
as key contributors to Antarctic primary production (e.g. Arrigo et al., 2016; Arrigo & van Dijken, 2003) and sea ice production
(e.g. Tamura et al., 2008; Nihashi, S. & Ohshima, 2015; Tamura et al., 2016) range from $\sim 1.3 - 6 \times 10^3 \text{ km}^2$, and many of these
polynyas are relatively narrow (10-100km). Thus, many of these biophysically critical polynyas cannot be resolved on the

25x25 km grid of the passive microwave satellite data (e.g. Special Sensor Microwave Imager [SSM/I]), much less on the
65 typically coarser $\sim 1^\circ$ ($\sim 100 \times 100$ km) resolution ESM grids. The challenge of identifying relatively smaller polynyas on
relatively coarser grids has been explored in observational data products with a polynya signature simulation method (PSSM;
Markus & Burns, 1995), which combines higher resolution 85GHz frequency data with the high contrast data of the 37GHz
channel to classify SSM/I data as shelf ice, open water or sea ice (rather than SICs) and from which polynya maps can then be
created at sub-pixel scales. This method has been applied to studies of marine productivity in Antarctic coastal polynyas (e.g.
70 Arrigo & van Dijken, 2003; Arrigo et al., 2015). Tamura et al. (2006; 2007) address the resolution problem by combining
SSM/I with the advanced very high-resolution radiometer data (AVHRR) to estimate sub-grid scale sea ice thickness (SIT) in
regions of thin sea ice. The resulting maps of sea ice thicknesses in thin sea ice areas along with reanalysis data from both the
European Centre for Medium-Range Weather Forecasts (ERA-40) and the National Centers for Environmental Prediction
(NCEP2) were used to make maps of sea ice production and variability in Antarctic polynyas (Tamura et al., 2007; Tamura et
75 al., 2015). This method of identifying thin sea ice areas was applied in work investigating the influence of icescapes on Emperor
penguin foraging habitat in East Antarctica (Labrousse et al., 2019).

The PSSM and sea ice production methods have been successfully used in identifying polynyas at sub-pixel scales in the
satellite data, yet they are not directly applicable to ESM data which is saved as grid-cell averaged quantities. Polynya studies
80 using ESMs thus use grid-cell averaged sea ice concentration (SIC) and/or thickness (SIT) thresholds to identify “polynya”
grid cells of lower and/or thinner sea ice than the surrounding grid cells (e.g. Mohrman et al., 2021; DuVivier et al., 2024) – a
method that has also been applied to satellite-based SICs (e.g. Massom et al., 1998; Duffy et al., 2024). These low sea ice grid
cells are then labelled polynyas, although strictly speaking they identify grid cells that have a polynya-like feature within them
per the given threshold rather than explicitly resolving individual polynya(s) within the grid cell. September Antarctic polynya
85 areas in CMIP6 models identified by SICs and SITs show particularly large inter-model spread in size and frequency across
all CMIP6 models, and differences in coastal polynyas are attributed at least in part to differences in horizontal resolution
although the impacts of different resolutions have not, to our knowledge, been explored (Morhman et al., 2021). ESMs compute
sea ice production directly, which in turn can identify regions of high-sea ice productivity and thus infer coastal polynya
regions – although resolution of these regions will still depend on the model grid (e.g. Joeng et al., 2023).

90 Satellite data and ESM output have different methodologies for determining SICs, which further complicate comparisons of
polynyas and/or polynya-like features identified in these products. Satellite SICs are retrieved from satellite microwave
radiometers using sea ice algorithms which differ in their sensitivity to sea ice temperature and emissivity, atmospheric
conditions (including winds, cloud liquid water vapor content, humidity), surface roughness in open water areas and the sea
95 ice state and presence of liquid water on the sea ice (e.g. melt ponds). Uncertainties in satellite-based SICs tend to be greatest
in summer season, and regions of low sea ice concentrations and thin ice (e.g. Meier, Windnagel and Stuart, 2021; Ivanova et
al., 2015 and references therein). Earth system model SICs, on the other hand, are based on the physical evolution of simulated

sea ice due to fluxes of energy and momentum. ESMs calculate SICs/SITs to very small fractions/thicknesses, albeit with potential biases from forcing or structural model uncertainty. Most ESMs use an ice thickness distribution (ITD) to represent the heterogeneity of sea ice thicknesses within a grid cell. The average sea ice thickness of a grid cell is calculated as the total volume of sea ice in the discrete thickness categories divided by the area of the grid cell. Satellite-derived SIT estimates are becoming more readily available, yet remain spatially and temporally limited compared to SICs, particularly in the Antarctic, and have considerable uncertainty compared with SIC products (e.g. Bocquet et al., 2024; Fons et al., 2022; Kacimi & Kwok, 2022; Zygmuntowska et al., 2014 and references therein). Thus, SIT from satellite products has limited capacity for identifying thin sea ice which may be relevant for polynyas, especially during the active ice-growth period of wintertime coastal polynyas. Further, ESM SICs and SITs are calculated at the model time-step (e.g. every hour) then averaged over a day for daily averages, whereas satellite microwave radiometer data represent an instantaneous snapshot of conditions specific to a particular time and location (typically daily or bi-daily; Meier et al., 2014).

ESMs are powerful tools for exploring past, present and future climates and how polar marine ecosystems may respond to climatic change, and satellite SIC data have been used extensively to validate sea ice areas and extents in ESMs. Earth system models (ESMs) are increasingly being used to study polynyas in the climate system (e.g. Mohrmann et al., 2021; Jeong et al., 2023; DuVivier et al., 2024) yet we are unaware of any publications that assess in detail how to best identify and compare climatologically relevant polynya-like features in both ESMs and satellite products. The following are the four primary questions we address in this work:

1. Are Earth System Models (ESMs) capable of capturing climatologically and biologically relevant coastal polynya-like features?
2. How to best use observational products to validate polynya-like features in ESMs?
3. Do polynya-like features in ESMs forced by reanalysis data occur in regions/areas where polynyas and polynya-like features are identified in observations?
4. Do coastal polynya features in ESMs function in marine ecological processes as they do in the real world?

We also seek to understand how choice of polynya metrics may influence results in terms of polynya areas, locations and trends. We intend for this exploration to give guidance on implications of various polynya metric choices for model and satellite-based data analysis. The role of low sea ice areas in Antarctic marine ecosystems is dynamic and diverse – polynyas affect availability of light and nutrients for phytoplankton, provide open water access and thus prey for marine predators such as penguins and seals, and the timing of low sea ice conditions influences the seasonal progression of phytoplankton blooms. In this paper, we investigate the impacts of metric choices on coastal polynya identification, compare polynya areas estimated from simulated and observationally based data, and assess if our polynya metrics identify biologically important marine regions in the climate model. This analysis provides comprehensive and quantifiable information on polynya identification that can

help guide future work to assess the role of changing polynyas on Antarctic marine ecosystem dynamics and the physical environment.

2 Data

2.1 Satellite observations

135 We consider two daily observational Climate Data Records (CDR) of gridded sea ice concentration data from satellite images:
version 4 of the CDR of passive microwave SIC developed at the National Snow & Ice Data Center (NSIDC) for the National
Oceanic and Atmospheric Administration (NOAA; Meier et al., 2014; Meier et al., 2021) and the European Organisation for
the Exploitation of Meteorological Satellites (EUMETSAT) Ocean and Sea Ice Satellite Application Facility (OSISAF) SIC
CDR (OSI-450) from 1979-2015 and the OSI-430-b from 2016-2020 (Lavergne et al., 2019). The NOAA data are a merged
140 product of the NASA Team (Cavalieri et al., 1984) and Bootstrap (Comiso, 1986) algorithms, with the higher SIC of the two
products used as the CDR value when the two products differ (Meier et al., 2014). The NOAA and OSISAF data are derived
from the same satellite radiometer data using different sea ice retrieval algorithms. The largest differences in SICs resulting
from different retrieval algorithms tend to be found in areas of relatively thin sea ice, where SIC tend to be underestimated
across all algorithms (Ivanova et al., 2015; Kwok et al., 2007; Grenfell et al., 1992). We include the NOAA and OSISAF
145 products of sea ice concentrations in this study to explore differences in identified polynya areas from observationally based
gridded SIC products that may result due to different sea ice retrieval algorithms. Both the NOAA and OSISAF CDRs are
used extensively in the ESM research community for model testing, validation and improvement.

We create polynya maps for the NOAA and OSISAF SIC products on both the original (25 km x 25 km) Equal Area Scaleable
150 Earth (EASE) grid as well as regridded onto a nominal 1° climate model grid, as described below. The reason to create polynya
maps on both grids is to better understand the impacts of resolution and spatially regridding on polynya identification across
different products (i.e. satellite observations and Earth System Models) that span large spatial scales. Additionally, given the
differences in instantaneous satellite observations and model average conditions, we apply our polynya metrics to daily and
monthly averaged data to better understand the impacts of temporal resolution on polynya identification.

155

2.2 Climate Model Output

This study uses output from a configuration of the Community Earth System Model Version 2 (CESM2; Danabasoglu et al.
2020) for representative ESM data. This hindcast simulation (JRA-CESM; Krumhardt et al., 2024) is a prognostic ice-ocean
simulation with CESM2 that is forced by the Japanese Reanalysis product (JRA; Kobayashi et al., 2015; Tsujino et al., 2018)
160 using reanalysis atmospheric conditions that match observed weather. This hindcast simulation removes model-observational
differences due to atmospheric forcing or internal variability and thus the simulated sea ice conditions and variability in the

JRA-CESM are more directly comparable to the satellite products. Antarctic SICs and sea ice extents (SIE; defined as the area covered by sea ice concentrations of 15% or higher) in the JRA-CESM compare well, spatially and temporally (Krumhardt et al., 2024), with the NSIDC Climate Data Record (Meier et al., 2021) and the NSIDC Sea Ice Index (Fetterer et al., 2017).

165 The JRA-CESM is on a standard nominal 1° grid and uses version 5 of the Los Alamos Sea Ice model (CICE5; Hunke et al., 2015) and the Parallel Ocean Program Version 2 (POP2; Smith et al., 2010) ocean model. CICE is a thermodynamic-dynamic model that uses an Ice Thickness Distribution (ITD) scheme with 5 thickness categories to parameterize sub-grid scale variations in ice thickness (e.g. Holland et al., 2006). The CESM2 computes light penetration based on this subgrid-scale sea ice thickness, important for capturing the non-linear photosynthetic function in ice-covered waters (Long et al., 2015). CICE5
170 simulates thermodynamic (growth and melt rates of snow and ice from vertical conductive, radiative and turbulent heat fluxes) and dynamic (including advection and ridging) changes to sea ice concentrations and volume (Hunke et al., 2013). Thermodynamics and dynamics operate on sea ice within each thickness category. Grid cell averaged sea ice thickness is calculated by taking the sum of the volume of sea ice in each thickness category and dividing by the area of the grid cell. The sea ice component of the CESM2 includes a “mushy” thermodynamic component that allows for a mixture of brine and solid
175 ice which leads to increases in both frazil ice production and Antarctic Bottom Water formation in polynya-like coastal features when compared with the earlier model version, the CESM1 (DuVivier et al., 2021; Singh et al., 2020). Coastal frazil ice production is particularly important in Antarctic coastal polynyas (e.g. Nakata et al., 2021 and references therein). The CESM2 hindcast simulations also use the Marine Biogeochemical Library (MARBL) model (Long et al., 2021), which simulates planktonic marine ecosystem dynamics and coupled cycles of carbon, nitrogen, phosphorus, iron, silica, and oxygen. MARBL
180 is highly configurable, allowing a flexible number of plankton functional types – for this study MARBL is a slightly more complex ecosystem (4 phytoplankton and 2 zooplankton functional types) than in standard configuration, as described in Krumhardt et al. (2024). We focus on net primary productivity (NPP) here, which is the sum of net carbon fixation by all phytoplankton functional types. This paper presents a more in-depth view of polynya-like features in the CESM2 than previous related work (DuVivier et al., 2021).

185 **3 Methods**

3.1 Polynya algorithm

Our algorithm defines polynyas from a particular variable and threshold value. The two physical sea ice variables we focus on for polynya identification are SIC (observations and model) and SIT (model). Polynyas are identified as contiguous groupings of grid cells that fall below a given threshold and are surrounded by land and/or ice-covered gridcells above the threshold (e.g.
190 Appendix A). This method cannot resolve discrete polynyas on scales smaller than an individual grid cell but rather identifies grid cells that contain higher fractions of open water (or thinner sea ice) compared to surrounding grid cells. Model output is on a grid cell average and does not contain information regarding the sub-grid scale distribution of open water within the grid

cell such as leads, polynyas, regions of new ice etc., and thus these areas are more accurately described as “polynya-like features” although we will continue to use the term “polynya” for brevity.

195

The first step in the algorithm identifies all grid cells that fall below the variable threshold and lie within the ice zone (i.e. not immediately bordering open ocean). In subsequent iterations, the algorithm checks neighbouring grid cells. If all grid cells bordering a region of ice below the threshold are bounded by higher threshold variables and/or land, then this region is identified as a polynya (or polynya-like feature, as noted above). If any neighbouring cells are bounded by open ocean, the grid cells are not considered a polynya even though they meet the threshold requirement. This iterative process is necessary in some regions and seasons when the northern ice edge may be complicated as polynyas open and merge with open water (e.g. in the Ross Sea in austral spring and around the Western Antarctic Peninsula with a relatively complicated coastline). The polynya algorithm also numbers individual polynyas and calculates individual polynya areas based on the number of grid cells each individual polynya occupies. In this manner, we can calculate not only total polynya area by region, but also the number of individual polynyas and their sizes. This threshold-based algorithm is similar to the method employed by Mohrmann et al. (2023), and we identify polynyas for a range of threshold values for satellite-based SICs and model-based SICs and SITs. Our algorithm maps both open-water (surrounded by higher concentrations or thicknesses of sea ice) and coastal (at least one grid-cell neighbouring land) polynyas, but this work focuses primarily on coastal polynyas because of their important ecological functions and because open ocean polynyas are relatively uncommon in observations and in the model results.

210

We first explore the influence of polynya metrics on polynya identification in the satellite and JRA-CESM data by calculating integrated “total polynya areas” (the area of grid cells containing polynya-like features) by region (Southern Hemisphere and smaller regions using the regional definitions of Parkinson & Cavalieri, 2012 and shown in Fig. 1f) for winter (June-July-August; JJA) and spring (September-October-November; SON). We focus on winter and spring as these seasons are key for formation of coastal polynyas as well as light and nutrient availability for marine productivity. We then choose one SIC and one SIT polynya threshold metric to apply to the satellite products and the JRA-CESM to explore spatial and temporal relationships between these different products at a given threshold. The thresholds chosen are based on results from the range of possible thresholds and represent a compromise with regards to number of polynyas and total integrated southern hemisphere (SH) polynya area. We aim for a total number of polynyas within the observational range, winter-spring, for sea ice production (13; Nihashi & Ohshima, 2015; Tamura et al., 2008) and high marine productivity (37-46; Arrigo & van Dijken, 2004; Arrigo et al., 2015). The total area of polynyas in our method represents the area of grid cells labelled as containing polynya-like features, and therefore we pick thresholds that lead to polynya-grid-cell-areas at least as large if not larger than the lower ranges of published observational estimates for these seasons ($\sim 1 \times 10^5 \text{ km}^2$; e.g. Arrigo & van Dijken, 2004; Arrigo & van Dijken, 2004; Tamura et al., 2008; Nihashi & Ohshima, 2015).

220

225 **3.2 Impacts of metric thresholds, spatial and temporal resolutions on polynya identification**

We apply a range of SIC (15%-85% by increments of 1%) and SIT (10-85 cm in increments of 1 cm) thresholds to identify polynyas in the two satellite products (“OBS”) and the JRA-CESM on different spatial and temporal resolutions. Polynyas often have scales and dimensions much smaller than that resolved by standard gridded sea ice data, even the relatively fine resolution OBS data on a 25km² EASE grid. Thus, appropriate threshold values for identifying polynyas may depend on the size of the data grid cell. As a simplified example, a polynya defined by a 10% SIC threshold on a 6.25 km EASE grid (e.g. the sub-pixel grid used by Arrigo & VanDijken, 2003) and surrounded by grid cells of 100% SIC would be classified as a polynya on 25/45 km EASE grids at 94/98% SIC thresholds (e.g. Appendix B). Polynya threshold choices are further complicated by climate model grids that tend to be in degrees latitude/longitude rather than equal-area grids. A given SIC threshold for an EASE grid is the equivalent of an area threshold (i.e. km² of open water within a grid cell), whereas on the equal-latitude/longitude grid a given SIC will correspond to different total open water areas within a grid cell depending on latitude (as the grid cell surface area is latitude-dependent, and thus a percentage of the total grid cell area will represent a different area depending on latitude; see Appendix B). Given these considerations and the scientific question at hand, the threshold used may need to depend on grid size and may be specific to region, season, and variable. We explore the impacts of grid size on polynya areas by making polynya maps from different grid sizes in the satellite data – the original 25 km EASE grid and regridded to the standard nominal 1° CESM grid. We compare polynya metrics between satellite and climate model output by focusing on the regridded satellite data.

Polynya-like features can change rapidly in time, particularly for wintertime Antarctic coastal polynyas when surface air temperatures are extremely cold and extensive (albeit thin) sea ice can form rapidly at open water surfaces. Polynyas identified from daily data, for example, may not appear on monthly time scales (particularly in the model, which can simulate high concentrations of very thin sea ice). We investigate the effects of temporal resolution on polynya identification by comparing polynyas estimated from daily and monthly data.

We calculate correlations between polynyas both within products and between products. We use the term “self-correlation” to refer to correlations calculated from the same product (e.g. polynya areas calculated using the NOAA CDR on the EASE grid correlated with those calculated from the NOAA CDR regridded to the model grid) and “cross-correlation” for correlations between different data sources (e.g. polynya areas identified using the OSISAF data and the model data).

3.3 Impacts of differing methodologies for calculating sea ice concentrations in the model and satellite images

Comparing polynya estimates in models and satellite observations is not a trivial matter. Uncertainties increase in the passive microwave retrievals of SIC at low concentrations, typically ~10% and lower. As a result, the NSIDC CDR implements a 10% minimum threshold on the CDR data product (Meier, Windnagel and Stuart, 2021). Satellite-based SICs are underrepresented

in areas of thin sea ice across all retrieval algorithms, particularly where sea ice thicknesses are below 25 cm (Ivanova et al., 2015). Sea ice between 5 and 20 cm thick will result in systematically underestimated SICs (Ivanova et al., 2015). In contrast, climate model simulations calculate SICs to very small fractions independent of mean SIT. This complicates how a polynya is identified in each dataset. For example, winter-time polynyas can be regions of extremely high sea ice production where sea ice forms nearly as fast as winds expose water to the overlying atmosphere. In these conditions, one might expect polynya metrics based on SIT would be more appropriate than SIC in model output as the extreme cold wintertime air temperatures can lead to nearly immediate sea ice formation and thus high SICs even if SITs are very thin. Conversely, SICs are underestimated in satellite products when the ice is very thin, so a satellite observation in these conditions should show lower SIC (note that observations of SIT are very limited). This is a clear example where SICs may be better suited for defining wintertime polynyas from satellite images whereas SITs might be a better metric from climate model output.

Given the challenges of passive microwave measurements and retrieval algorithms to estimate sea ice concentrations in low concentration and thickness conditions, as detailed above, we explore the influence of different definitions for SIC in satellite-based observations and model output by degrading the JRA-CESM hindcast sea ice concentrations such that the modified SICs more closely align with SICs as they would be if remotely sensed. Model SICs are degraded by setting daily SIC in grid cells with less than 10% SIC or less than 5 cm daily SIT to 0% SIC, closer to the values that a satellite would observe in these conditions. Daily SICs within grid cells that have SITs of 5-20 cm thick are set to half of the original model SIC output, corresponding to the underestimation of ice concentration over thin ice by satellites (Appendix C). Although using daily averaged data is not the same as the instantaneous satellite-snapshot data, it is the highest frequency model output of sea ice data available. We compare the degraded model SIC to the original output to gain insight into how differences in SIC methodologies may impact polynya identification in both observed and model data products.

3.4 Influence of metrics and resolutions on polynya identification

One of our primary goals in this work is to better understand how different metric choices on a variety of gridded data products will influence polynya identification, and how to best compare polynyas identified in both observational and simulated data for model validation purposes. We explore both the influence of resolutions (temporal and spatial) and metric thresholds. We identify polynyas over a range of SIC thresholds (15%-85%) in the satellite-based observations on the original EASE grid, regridded to the nominal 1° model grid, and for both daily and monthly-averaged data. Similarly, we apply the same range of SIC thresholds as well as a range of SIT thresholds (10-85 cm) to the daily and monthly JRA-CESM. We analyse these results for winter and spring, and on regional and hemispheric scales to elucidate how the influence of polynya identification metric choice may differ by season and region. Based on the analysis of the NOAA and OSISAF CDRs and JRA-CESM, we pick two polynya identification metrics (85% SIC and 0.4 cm SIT thresholds on monthly averaged sea ice data) to further explore similarities and differences in resultant temporal and spatial polynya area time series of the two satellite-based data products

and the JRA-CESM to highlight impacts of temporal and spatial regridding, different observational data product choices, and
290 model-observational comparison.

3.5 NPP and polynyas

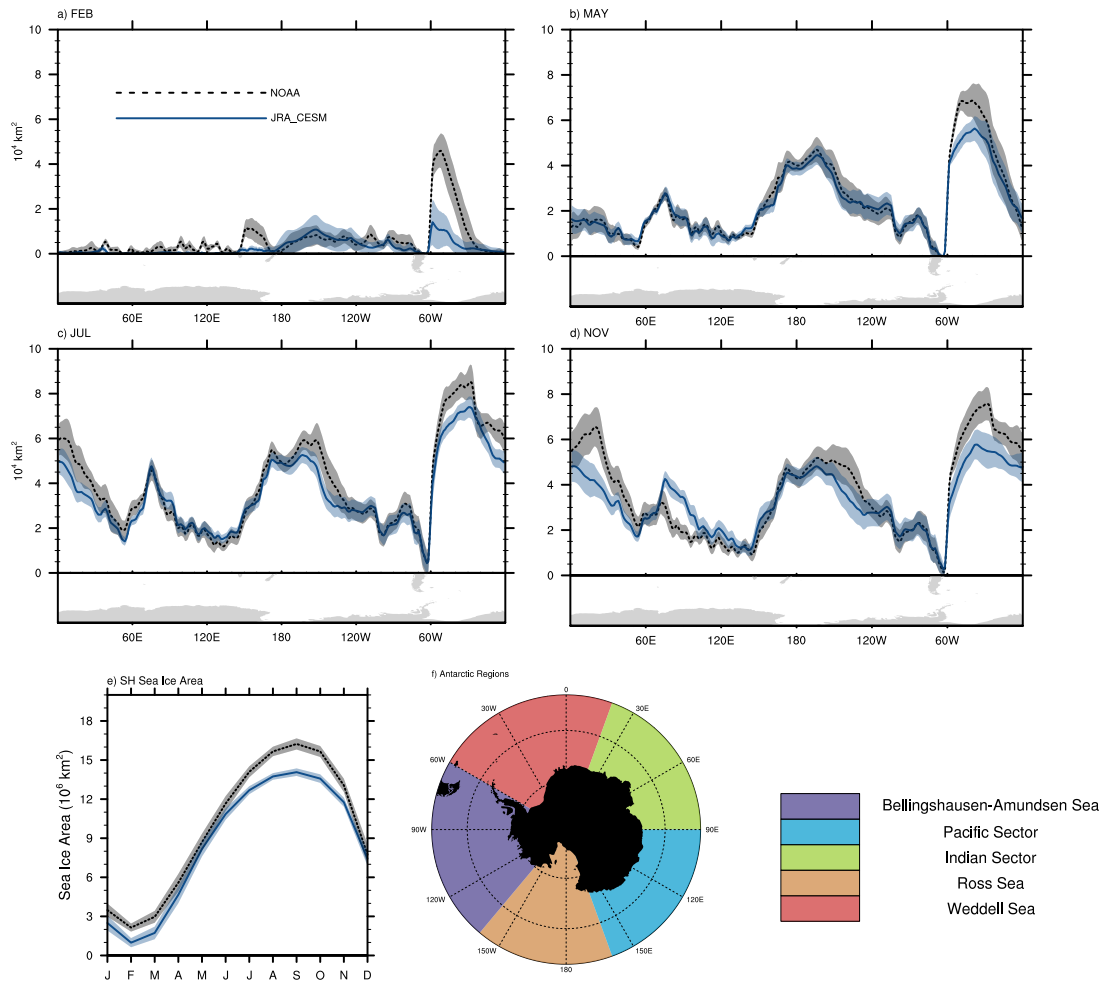
Polynyas play important roles in physical and biological processes, and optimal metrics for defining polynyas may differ
depending on analytical goals. Here we explore what constitutes an optimal model-derived polynya metric based on their
ecosystem-relevance, specifically their relation to NPP. During the austral spring (September-October-November), sea ice is
295 melting and directly impacting NPP through light availability. During this season the optimal choice of metric (SIT or SIC) to
define polynyas is not clear, and as such we pick one metric based on SIC and another on SIT to identify polynyas and
investigate if these springtime polynya areas have increased productivity in the JRA-CESM model simulations by calculating
NPP both within the polynya areas and within the sea ice zone (SIZ) as a whole. The SIZ is defined as the region south of the
mean wintertime (June-July-August) northern pack ice ($SIC \geq 85\%$) boundary. Thus, regions within the ice pack and near the
300 coast that may have lower sea ice concentrations or ice thicknesses (i.e. “polynyas”) lie within the SIZ. The goal is to help
inform choices in future studies particularly when using model output that may not include marine biology components or that
do not allow for trophic transfers to higher trophic levels as is critical for high latitude, light-limited systems.

4 Results

4.1 Large-scale sea ice properties

305 The CESM2 captures observed Southern Hemisphere (SH) sea ice area climatology as well as temporal and spatial variability
quite well compared to CMIP6 models (e.g. Roach et al., 2020). Additionally, the CESM2 simulates coastal polynya-like
features of high sea ice production (Singh et al., 2020; DuVivier et al. 2021). The CESM2 hindcast, forced by atmospheric
reanalysis, underestimates total SH sea ice areas (SIA) from July through October by ~10-14% ($\sim 1.4\text{-}2.6 \times 10^6 \text{ km}^2$) compared
with both the NOAA and OSISAF products (Fig. 1e; NOAA and OSISAF sea ice areas are very slightly different –
310 Supplemental Figure 2 – so only the NOAA CDR is shown in Fig. 1). Regionally, the JRA-CESM tends to underestimate
Antarctic sea ice in the Weddell Sea for all months of the year and in the Indian sector in the winter through spring months
(Fig. 1 and Supplemental Fig. 1).

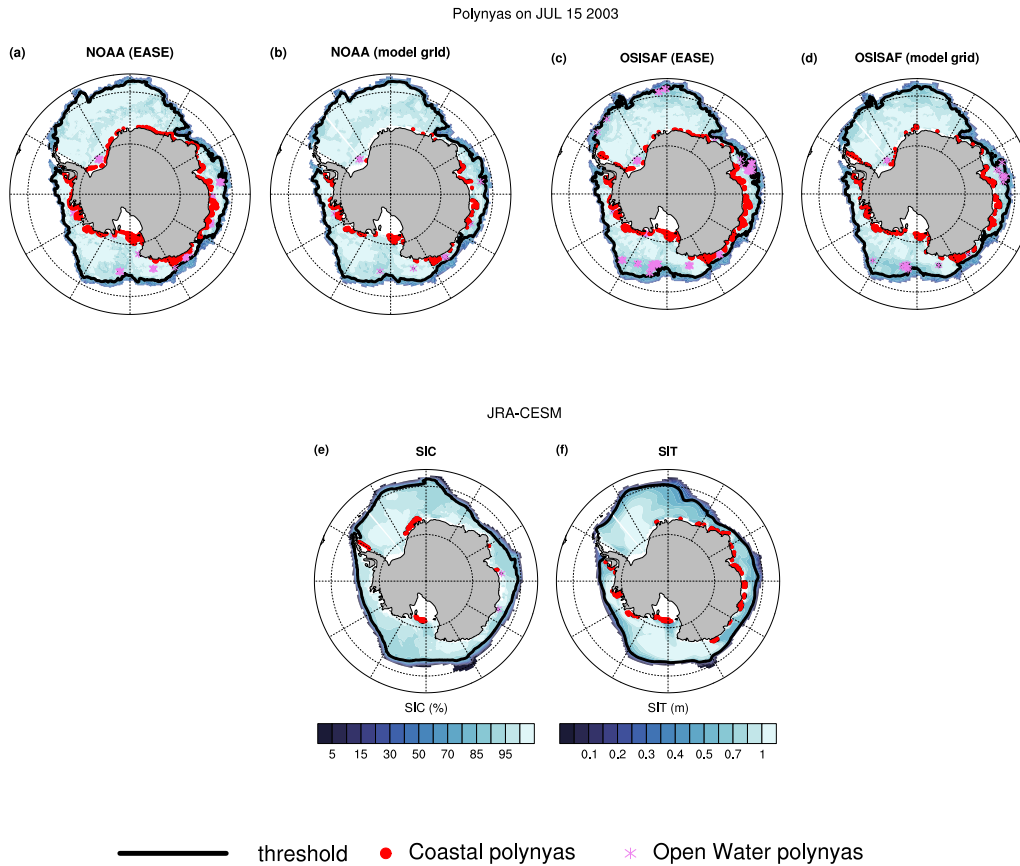
1979-2020 Mean Sea Ice Area



315 **Figure 1. 1979-2020 Monthly mean total sea ice area as a function of longitude for a) February, b) May, c) July, d) November, e) monthly Southern Hemisphere (SH) sea ice area climatology for the NOAA CDR (black) and JRA-CESM (blue); and f) Antarctic regions map. Thick dashed (NOAA) and solid (JRA-CESM) lines indicate the mean; shaded polygons indicate the mean ± 1 standard deviation. Sea ice areas as a function of longitude have been smoothed by a 3-point running average.**

4.2 Polynyas in the satellite data

320 Maps of open water and coastal polynyas on July 15, 2003, calculated using our algorithm and a SIC threshold of 85% for observational datasets are shown in Fig. 2 (a-e). Note that this date is not special, but a representative day shown to illustrate differences in polynya identification metrics across products. We picked a random winter day as relatively few polynyas are identified in January-April in all data products, and the broad similarities and differences between polynyas identified in different data products on this winter day are typical.



325 **Figure 2. Polynya maps for July 15, 2003, using SIC 85% threshold for the NOAA and OSISAF CDR data on the original Equal Area Scaleable Earth (EASE) grid (a, c), the NOAA and OSISAF data regrided to the CESM grid (b, d), the JRA-CESM (e) and the JRA-CESM using a 0.4m SIT threshold (f). Open water and coastal polynyas are indicated by the pink stars and red dots. The 85% SIC and 0.4m contours are indicated by the thick black contours over the colour contoured SIC or SIT values. Sea ice concentrations below 15% are masked out.**

330

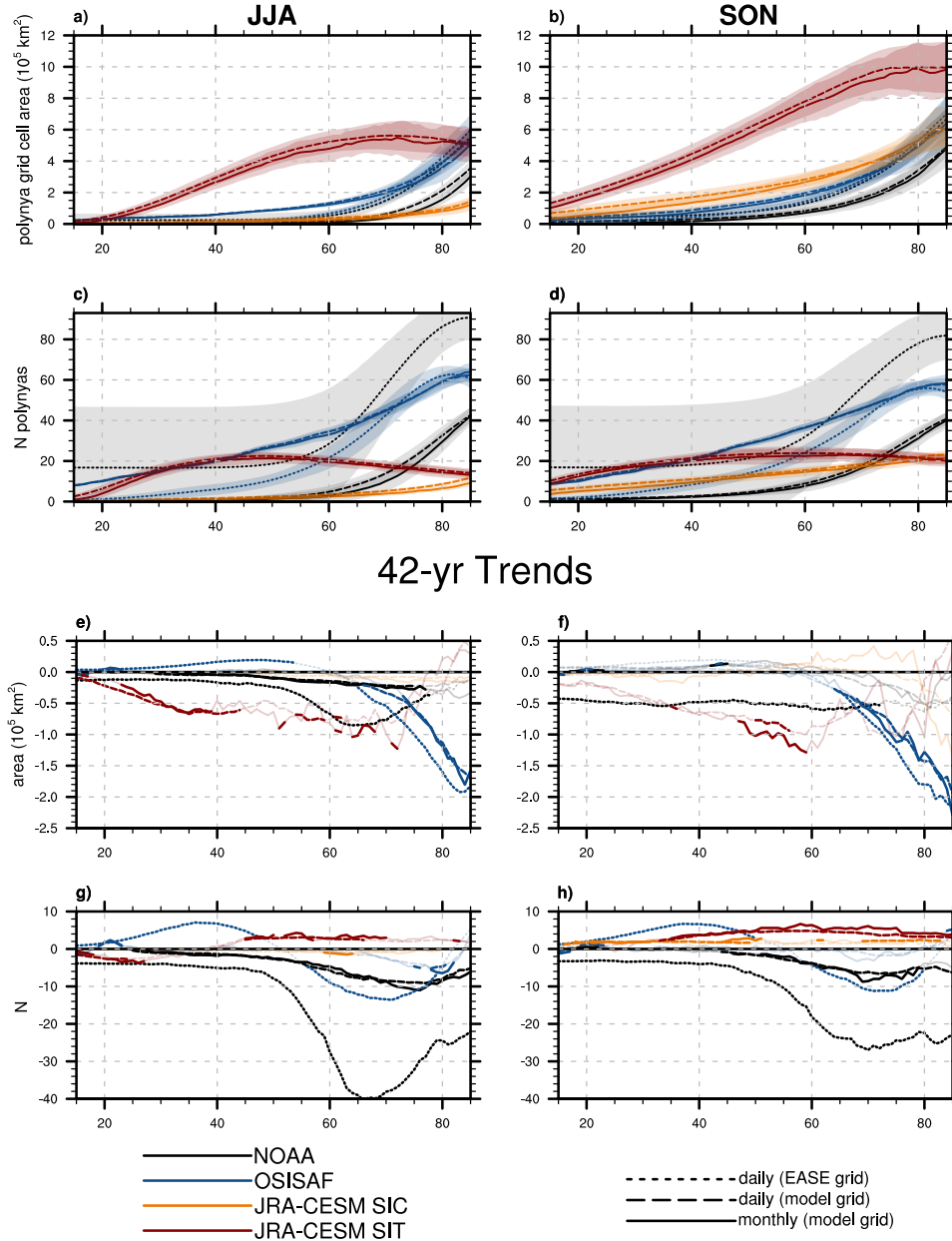
The sea ice edge (defined as the 15% SIC contour) is nearly identical for both the NOAA and OSISAF satellite products on the original grid and after regriding to the nominal 1° climate model grid (Fig. 2a-d). More open water polynyas are identified in the OSISAF product than in the NOAA product. Differences in coastal polynyas identified in the two satellite products are more mixed, with more coastal polynyas identified on the east side of the Antarctic peninsula in the OSISAF CDR than in the NOAA CDR, regrided or not, yet more coastal polynyas are identified in the Weddell Sea in the NOAA product than in the OSISAF product on the EASE grid. Regriding has a greater impact on polynya areas in the NOAA product than on the OSISAF product (Fig. 2 a-e and Fig 3 a-d). We show both open water and coastal polynyas identified in our example day, however we focus on coastal polynyas for the remainder of this study.

335

4.2.1 Southern Hemisphere polynya statistics in satellite based products

340 When moving beyond an example day and looking across all years, regriding the observational products from the original
EASE grid to the model grid has a larger impact on both number and area of polynyas identified in the NOAA product than
for the OSISAF product (Figure 3a-d). The climatological winter and spring polynya areas and number of polynyas at a given
SIC threshold in both observational products show only small changes when using monthly vs daily data (after regriding to
the model grid). Integrated southern hemisphere (SH) coastal polynya areas as well as number of polynyas are larger in the
345 NOAA product when identified on the original finer-resolution EASE grid than when regrided to the 1° CESM grid in both
winter and spring across the full range of SIC thresholds. Polynya areas in the regrided NOAA product are nearly the same
using both daily and monthly averaged data. On the other hand, regriding the OSISAF data to the model grid leads to larger
polynya areas and higher numbers of polynyas at SIC thresholds below ~70%, with smaller differences (within 1 standard
deviation range of polynyas identified on the EASE grid at daily resolution) higher thresholds. Like in the NOAA data, the
350 differences in the climatological polynya areas and numbers between regrided daily and monthly data are quite small (Figure
3 a-d; see Supplemental Figure 3 for summer, DJF, and fall, MAM). Although integrated SH polynya areas are nearly identical
across a range of thresholds from both satellite products on the original EASE, daily grid, regriding has opposing impacts on
polynya identification in the two satellite products. After regriding to the model grid, consistently higher polynya areas and
numbers are identified in the OSISAF data than from the NOAA data for both seasons and across the entire range of thresholds.
355 Variability in SH polynya areas tends to be larger during the spring, particularly at high SIC thresholds, and continue to increase
into the summer as areas of low/thin sea ice within the icepack merge with surrounding open ocean as the sea ice melts and
contracts (Supplemental Figure 3).

SH coastal polynyas (1979-2020)



360 **Figure 3.** Total SH mean (1979-2020) coastal polynya areas (a-b), number of polynyas (c-d), 42-yr trends in polynya areas (e-f) and 42-yr trends in number of polynyas (g-h) as a function of threshold value (SIC, SIT) for winter (JJA; left column) and Spring (SON; right column) for NOAA (black), OSISAF (blue), and JRA-CESM (SIC metric, orange and SIT metric, maroon). X-axis units are 15-85% for SIC and 15 - 85 cm for SIT. Polynyas identified using the daily observational data on the original EASE grid are shown by dotted lines; dashed/solid lines indicate polynyas identified using daily/monthly data on the model grid. Climatological mean

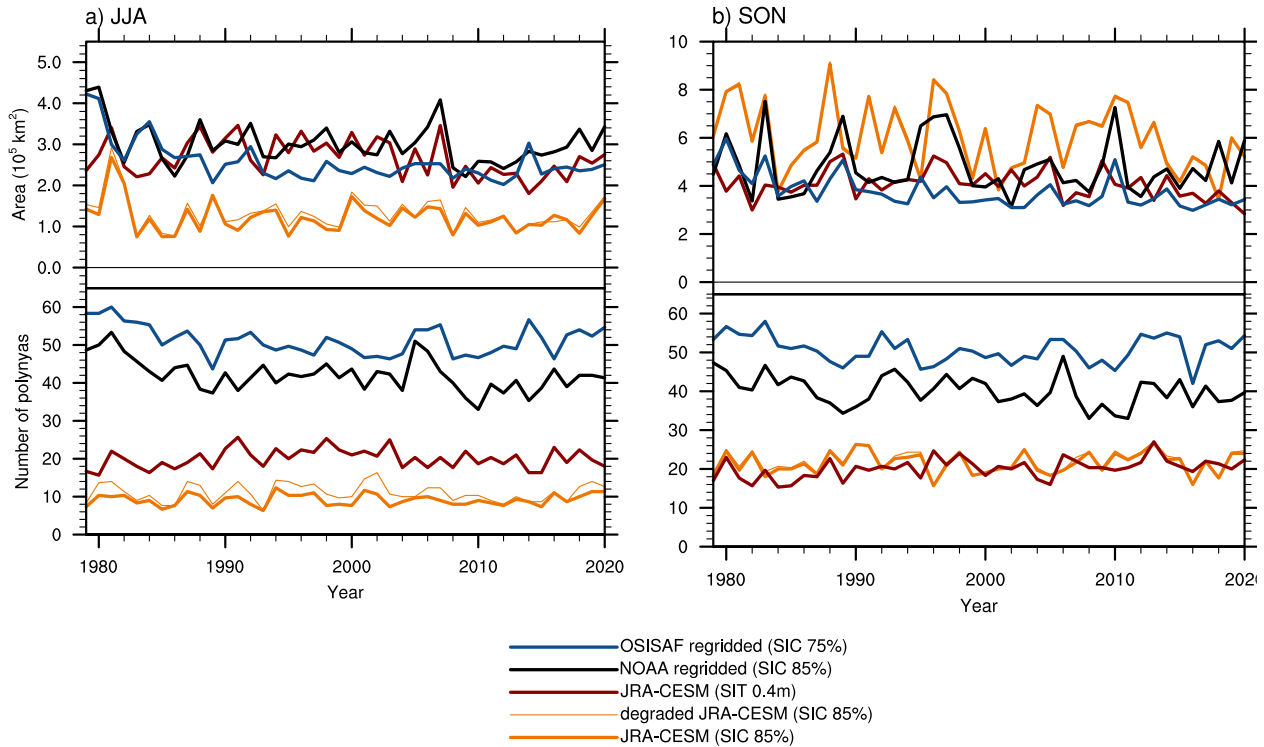
365 (1979-2020) values are shown in the thick lines; ± 1 standard deviations shown by the lighter shading (a-d). Dark, thick
370 dots/dashes/lines in the trend figures (e-h) indicate 95% or higher significance based on the Mann-Kendall non-parametric trend
significance (Mann 1945; Kendall 1975; Gilbert 1987).

Trends in polynyas identified in the observational products differ by retrieval method, SIC threshold and spatial and temporal
370 grids. Significant negative trends (and no significant positive trends) are seen for the NOAA daily CDR on the EASE grid in
both seasons across all SIC thresholds for the number of polynyas, and at SIC thresholds less than $\sim 76\%/72\%$ for the JJA/SON
integrated polynya areas. On the other hand, polynyas identified in the OSISAF product show significant positive trends in
area (JJA) and number (JJA, SON) at low SIC thresholds, and significant negative trends at high SIC thresholds (SH polynya
375 areas and numbers, both seasons). After regridding to the model grid, integrated SH polynya trends are negative and significant
only in the winter and at SIC thresholds **lower** than $\sim 75\%$ in the NOAA product and significantly smaller in magnitude (up to
 ~ 3 -fold), and yet negative in both seasons in the OSISAF product and at SIC thresholds **higher** than $\sim 65\%$. These
inconsistencies in trends across thresholds, observational data products and grids are also apparent in the regionally integrated
timeseries except for the Bellingshausen-Amundsen sea region which shows significant negative trends in polynya areas for
both CDRs, on both the EASE and model grid, across a range of thresholds for the winter season (Supplemental Figures 4-8).

380

To better illustrate and compare relationships between polynya areas, numbers and locations, we show in more detail polynyas
identified in observational and model data at select SIC and SIT (model) thresholds. We pick threshold values such that the
resultant seasonal coastal polynya areas and numbers are consistent with published work (e.g. Arrigo & Van Dijken, 2003;
Arrigo et al., 2015; Tamura et al., 2008; Nihashi & Ohshima, 2015), as outlined in our methods section, and such that integrated
385 SH polynya areas are roughly equal in both seasons between all data sources and grids. We recognize that there is not one
clear choice of metrics and therefore our thresholds are somewhat arbitrary. Alternative threshold choices we have tried do not
change our results (not shown). The metrics and thresholds we use for the satellite products are SIC threshold values of 78%
for the EASE daily and 85% for the regridded NOAA (daily and monthly) data, and 75% for the OSISAF (all grids). Although
in general the integrated SH polynya areas are very similar between these metric choices in these data products, there are some
390 small differences in areas, numbers of polynyas, and variabilities (Figures 3a-d, 4). Notably, a larger number of distinct
polynyas are consistently identified in the OSISAF data than in the NOAA data (regridded to the 1° grid and monthly
averaged), and thus even though the SH polynya areas are quite similar, the average polynya size in the OSISAF is smaller
than in the NOAA product.

SH coastal polynyas 1979-2020

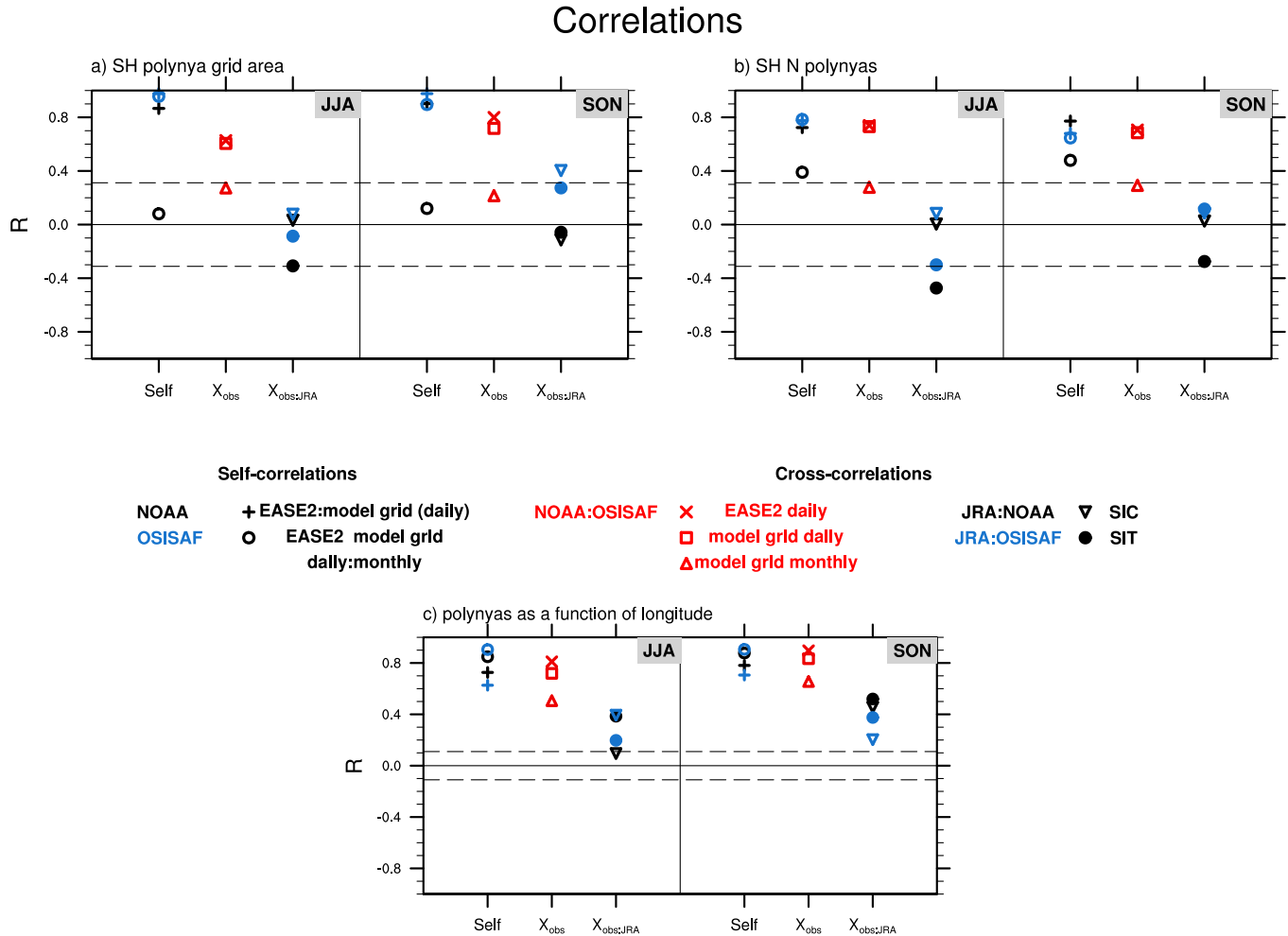


395

Figure 4. Southern Hemisphere (SH) 1979-2020 winter (JJA; a) and spring (SON; b) mean coastal polynya area (top panels) and number of individual polynyas (bottom panels). Polynya timeseries are for monthly NOAA (SIC 85%; black) and OSISAF (SIC 75%; blue) CDR data regridded onto the CESM grid, JRA-CESM model simulation using monthly SIC (85%; orange) and SIT (0.4m; brown), and the JRA-CESM model SIC degraded to more closely mimic satellite SICs (85%; orange thin line).

400 Correlation coefficients reveal impacts of regridding (spatially and temporally) as well as relationships between the two observational products (Figure 5). Regridding then monthly averaging the SICs before identifying polynyas results in a significant loss of self-correlation within the NOAA product, particularly for integrated SH polynya areas. Notably, timeseries of SH polynya areas from the daily data on the EASE grid and from the regridded, monthly averaged grid are not significantly self-correlated for either season for the NOAA data product. Cross-correlations for polynyas identified from the two
 405 observational products are significant only for polynyas identified from daily data (EASE and model grids), however the SH polynya timeseries (both areas and numbers) are not significantly cross-correlated between the observational products after regridding and monthly averaging. Self- and cross-correlations are comparable for the number of polynyas identified from the daily data (Figure 5b). Additionally, the cross-correlation coefficients between the daily observational products, although

410 significant, are ~ 0.7 (area) to ~ 0.75 (N), suggesting considerable variability in the time series due to the nuances of the retrieval algorithms.



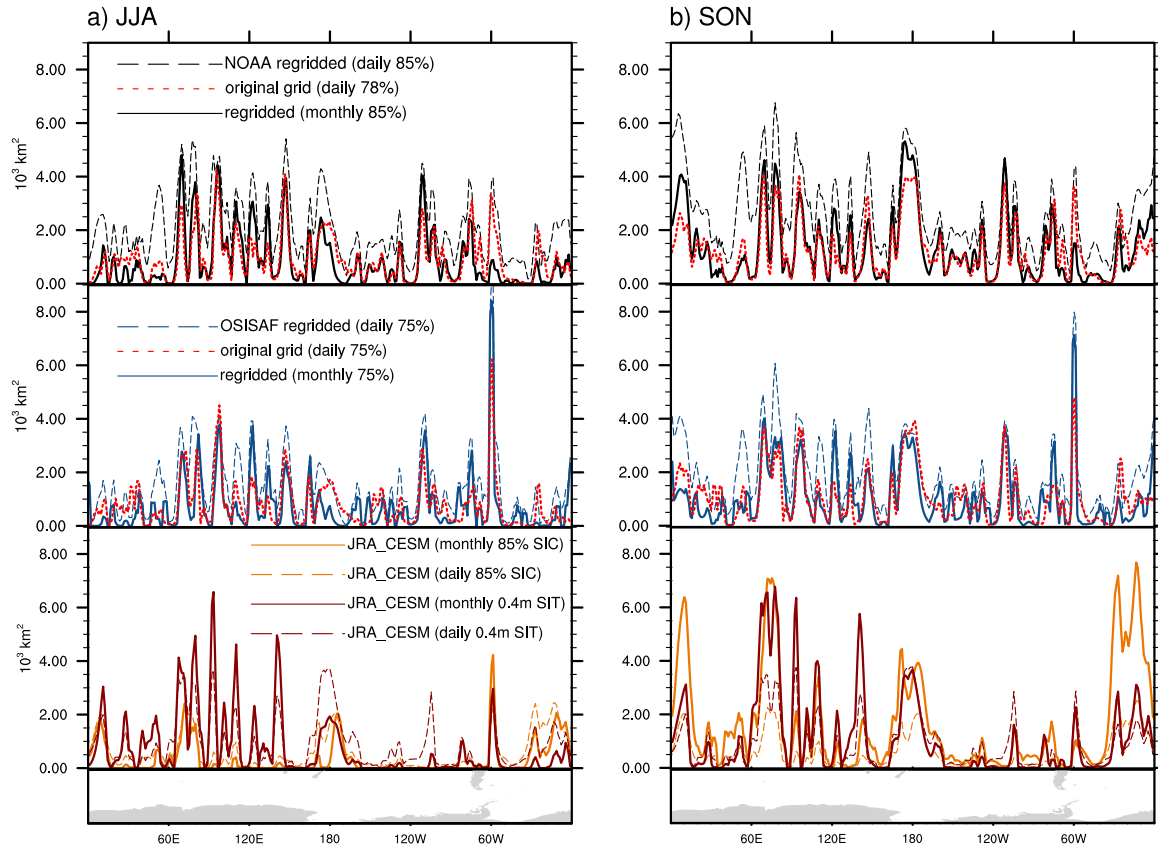
415 **Figure 5. Correlation coefficients for integrated SH polynya areas (a), number of polynyas (b) and polynyas as a function of longitude (c) for each JJA (left) and SON (right). Self-correlations are calculated between different grids (“regridding”) for same observational product (NOAA black; OSISAF, blue); cross-correlations between the two observational products (NOAA:OSISAF, red) and between the observational products and the JRA-CESM (obs:JRA; NOAA black; OSISAF, blue). Symbols show correlations between time/longitude polynya time series from the daily observational data on the original EASE grid vs daily (+) and monthly (o) regridded on the model grid; NOAA:OSISAF on the EASE grid (x) and then regridded daily (□) and monthly (open triangles); and between JRA-CESM polynyas identified using SIT 0.4 m (●) and SIC 85% metric (inverted open triangles). Dashed horizontal lines in a-c indicate the 95% significance level based on the Mann-Kendall non-parametric trends significance (Mann 1945; Kendall 1975; and Gilbert 1987).**

420

4.2.2 Regional polynyas in the satellite data

Winter (JJA) and spring (SON) polynya areas as a function of longitude show both similarities as well as differences resulting from choice of CDR (NOAA vs OSISAF), temporal (daily vs monthly) and spatial grids (EASE vs model; Figure 6). Higher polynya areas are identified, for example, by the NOAA data in the Ross Sea region and near the Antarctic peninsula in the OSISAF product. In general, polynya areas identified using the regrided daily product are higher in both CDRs than those identified using the daily data on the EASE grid or the monthly regrided data.

Latitudinal mean coastal polynya area (1979-2020)



430 **Figure 6. Winter (JJA; a) and summer (SON; b) mean coastal polynya area as a function of longitude for the NOAA CDR (top), OSISAF CDR (middle) and JRA-CESM (bottom). Polynya area as a function of longitude is shown as a 3° (longitudinal) running average. Top and middle panels show polynya areas for the three different grids and metrics - daily NOAA (78% SIC) and OSISAF (75% SIC) on the original grid (red dotted lines), CDR daily data regrided onto the CESM grid (NOAA 85% SIC black and OSISAF 75% blue) dashed lines, and regrided and monthly averaged (NOAA 85% SIC, black and OSISAF 75%, blue) solid lines.**

435 **Bottom panels in a) and b) show polynya areas based on JRA-CESM model simulation using different polynya thresholds: monthly (solid lines) and daily (dashed lines) SIC at 85% threshold (orange) and monthly SIT at 0.4m (brown) thresholds.**

Regridding and monthly averaging SICs from the CDRs has lower impact on spatial self- and cross-correlations than on the SH integrated temporal correlations (Figure 5c). Climatological, coastal polynya areas as a function of longitude from the OBS
440 data products show significant self- and cross-correlations regardless of temporal resolution or spatial grid and are generally higher than the temporal correlations. Unlike the temporal self-correlations, the longitudinal self-correlations are higher for polynyas identified on the monthly-averaged regrided data than for the daily regrided data.

Cross-correlations on regionally integrated timeseries are significantly correlated between the two observational data sources
445 after regridding and monthly averaging only in the winter season in the Bellingshausen-Amundsen sea and the Indian sector ($R \sim 0.4-0.5$, respectively; Supplemental Figure 9). In all other regions and in these regions in the spring, polynya areas and numbers estimated from the regrided and monthly averaged observational data products are not significantly cross-correlated (Supplemental Fig. 9). Self-correlations tend to be higher for polynya areas rather than polynya numbers, and the NOAA self-correlations after regridding and monthly averaging (original EASE grid, daily; model grid monthly) are insignificant for all
450 seasons and regions, except winter in the Bellingshausen-Amundsen sea.

Regional trends in polynya areas, when significant, are generally negative for both seasons with the exception of the Pacific sector, which has only significant positive trends at high SIC thresholds for both seasons, and in the Indian sector where significant trends are generally positive in both NOAA and OSISAF for SIC thresholds below $\sim 80\%$ (JJA) or 55% (SON), and significantly negative in the OSISAF at SIC thresholds above $\sim 80\%$ (JJA)/ 73% (SON; Supplemental Figures 4-8).

455 **4.3 Polynyas in the JRA-CESM vs NOAA and OSISAF OBS**

4.3.1 Integrated Southern Hemisphere polynya area

Polynya-like features have been found in CESM2 (DuVivier et al., 2021; Singh et al., 2020), and the CESM2 reproduces many characteristics of Antarctic sea ice quite well, making it a suitable model for closer investigation of polynya-like features. Polynyas identified in the model and the observations may disagree if the model doesn't adequately capture mechanisms for
460 producing polynyas, or due to model bias, or both. It is also possible that identification of polynyas in model output may require different metric choices than those used to identify polynyas in satellite products due to differences in model vs satellite data as outlined above.

Polynya maps for the example day, July 15, 2003, show how the 85% SIC threshold identifies far fewer polynyas in the JRA-
465 CESM than either the NOAA or the OSISAF CDRs (Fig. 2), suggesting that SIC may not identify polynya-like features in model output in the winter season. Indeed, monthly climatological (1979-2020) wintertime (JJA) SH polynya areas remain

very small in the JRA-CESM across the full range of SIC thresholds (Fig. 3; summer and fall are shown in Supplemental Fig. 3). During winter freeze up, open water can freeze very quickly in the model, resulting in high SICs and yet relatively thin SITs. Monthly climatologies of SH polynya area reveal that SIT thresholds, unlike SIC thresholds, identify large areas of wintertime coastal polynyas across a range of SIT thresholds (Fig. 3). Both integrated SH polynya areas and numbers are nearly the same regardless of whether they are identified in the model output using daily or monthly data.

To compare with polynyas identified in the observational products, we use polynyas identified in the JRA-CESM using thresholds of 85% SIC and 0.4m SIT (and we show results in Supplemental Figures 10-11 using a SIC threshold of 50% SIC and SIT of 0.2 m for comparison). Figure 4 shows time series of SH polynya area and total number of SH polynyas for winter and summer, and underscores many of the complications comparing polynyas estimated from satellite products to those estimated using climate model output on a seasonal basis. There are significant seasonal differences in polynyas identified using these two metrics: polynya areas identified using the SIT metric are roughly three times as large as those identified using the SIC metric (and much closer to the SH polynya areas in both OSISAF and NOAA CDRs) for winter (JJA), whereas the magnitude of SH polynya area is similar using these thresholds in the spring (SON; Figure 4). Fewer discrete polynyas are identified in the JRA-CESM using both SIT and SIC metrics than in either observational product in both seasons, even though the polynya areas are similar and thus the average polynya size will be smaller in the observations than in the model.

Temporal cross-correlations for SH polynya area, 1979-2020, between the NOAA, OSISAF and JRA-CESM are significant only between the OSISAF and the JRA-CESM using the SIC metric in the spring (SON; Fig. 5) – although it is interesting to note that the cross-correlations between regridded, monthly NOAA and OSISAF polynya area or number time series are not significantly correlated in either season. Trends (1979-2020) in SH polynya area in the JRA-CESM are significant and negative only for the polynyas identified by the SIT metric, and for a limited range of thresholds in both winter and spring (Fig. 3).

4.3.2 Regional polynya areas

Integrated mean SH polynya areas are very similar between the observational and model data for the metrics used, yet there are subtle regional differences. For example, climatological integrated SH polynya areas show very little difference whether using daily or monthly data (e.g. Figure 3), and yet the longitudinal maps reveal that the daily SIT data identify more wintertime polynyas than the monthly SIT data in the Ross and Bellingshausen-Amundsen seas (Fig. 6). Wintertime polynyas in the Bellingshausen-Amundsen sea are particularly anaemic using the 85% SIC metric (daily and monthly). In contrast, in spring (SON) the SIC threshold identifies higher modelled polynya areas in this region and they are closer to the polynya areas identified in the NOAA and OSISAF. Like the cross-correlations between the polynyas in the observational products, spatial cross-correlations between polynyas in the model and the observations are higher than temporal ones. Spatial cross-correlations between polynya area as a function of longitude identified in the satellite products and the JRA-CESM polynya area significant

and positive for both metrics (SIT, SIC) and both observational products (NOAA, OSISAF) in the spring (SON), and SIT
500 (NOAA, OSISAF) and SIC (OSISAF) in the winter (JJA; Fig. 5).

Regional trends are generally not significant in the model for most SIT and SIC thresholds (Supplemental Figs 4-8), although
there are some regionally significant trends for the SIT (0.4) metric, both negative (SIT: Ross, JJA; Weddell JJA and SON)
and positive (SIT: Bellingshausen-Amundsen Sea, SON) as well as significant negative trends in wintertime Indian sector
505 polynyas identified using the SIC metric.

4.4 Impacts of different definitions for sea ice concentrations in the model and satellite data

Discrepancies between polynyas identified using SIC in the model and the observational data may arise due to differences in
SIC definitions in satellite-based versus model data, particularly during the winter months. As discussed above, sea ice can
form immediately in the model during the cold austral expansion season and through the winter, thus resulting in SICs that are
510 high even though the ice may be very thin. Satellite imagery cannot differentiate between water and sea ice at very low SICs
or low sea ice thicknesses. To understand potential impacts that these model and observational differences in SICs may have
in polynya identification metrics, we degrade the model SIC output to more closely mimic satellite estimates of SIC. In areas
of low (<10% SIC) or thin (<5cm SIT) ice, we set daily SICs to 0% SIC, and in thin ice areas (5-20 cm SIT) the originally
modelled SICs are reduced by half. We then identify polynyas using an 85% SIC threshold on the degraded model output.

515

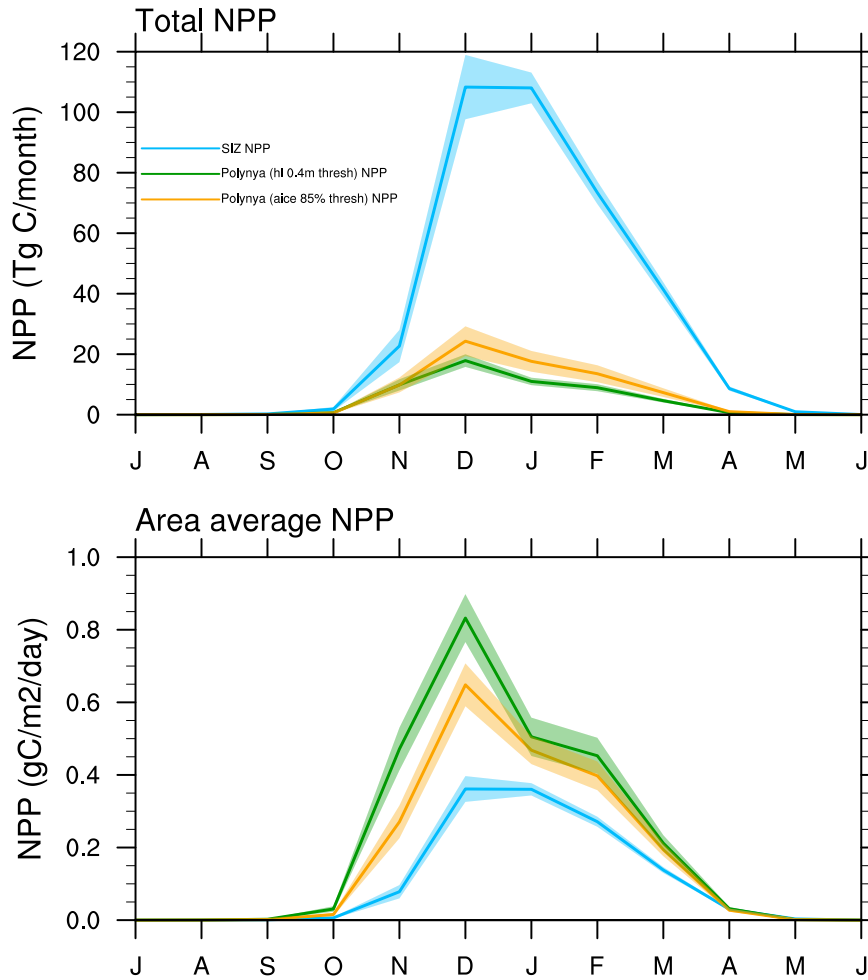
Comparisons of the standard model to degraded output indicate that degrading SICs results in small, positive differences that
are largest within the ice pack during ice growth season and along the ice edge in the winter (Fig. 4 and Appendix C);
differences from degraded output during the sea ice retreat season (SON) are much smaller with no discernible patterns (not
shown). Degrading the model data results in lower SICs throughout much of the fall pack ice and along the winter sea ice edge,
520 and these differences show very little regional variability and do not consistently explain the model bias of the non-degraded
data compared with the satellite products and in some cases would further increase model-observational biases. Identifying
polynyas based on the degraded model data (using an 85% SIC threshold) results in an increase in wintertime polynyas by
~10-20% (Figure 4 and Supplemental Figures 12-13). This increase is quite small compared to the model (using the SIC
threshold) versus CDR polynya area differences. Thus, it does not explain the differences in polynya areas estimated from
525 these three products and we focus on results using the standard model output (non-degraded) for the remainder of this paper.

4.5 Relationships between polynyas and NPP in the JRA-CESM

Net primary productivity (NPP) describes the rate of photosynthetically fixed carbon in the upper ocean; it quantifies the
energy available for marine food webs. In the high-latitude Southern Ocean, NPP increases markedly as the sea ice retreats
and light returns to Antarctic waters (e.g. Richert et al., 2019 and references therein). Light reaches the surface sooner in
530 polynyas than the surrounding ice-covered areas, relieving phytoplankton of light limitation (e.g. Arrigo & van Dijken, 2003).

We look at polynya regions defined in the austral spring (SON), to see if the model captures high NPPs within identified polynyas during the early growth season as is found in observations. The choice of metric (concentration or thickness) to identify SON polynyas in the model is not clear based on the previous analysis that indicates not only differences between the two observational products with respect to polynya areas, temporal and spatial correlations and trends, but also that polynyas identified in the JRA-CESM using a 0.4 m SIT and 0.85% SIC thresholds each have seasons and/or regions that better correlate with the NOAA or with the OSISAF. We therefore use austral spring polynya regions as identified by both the 0.4 SIT and the 85% SIC metrics for the NPP analysis.

Comparing the monthly average NPP per unit area within austral springtime coastal polynyas and within the sea ice zone allows us to better understand how polynyas may augment austral spring NPP and thus play a critical role in the Antarctic food web (Figure 7). Note that the SIZ, which is defined as the area covered seasonally with sea ice (as determined by the 1979-2020 mean winter - JJA - 85% SIC contour) covers significantly more ocean area than the spatial area of polynyas, so the net production within the SIZ is larger than in polynyas (Figure 7, top). However, we find that the NPP per unit area is substantially higher during the austral spring in regions identified as polynyas using both SIC and SIT polynya identification methods than it is within the SIZ in general (Figure 7, bottom). This finding suggests that the model does indeed capture high productivity within low and/or thinner ice regions. Additionally, the higher NPP per unit area persists into the summer and early spring (December-March) as well. Polynyas have a particularly large impact on NPP during December, when area average NPP within polynyas is more than twice as much as within the SIZ when using the 0.4m SIT threshold and 1.5x higher when using the 85% SIC threshold. Although the total integrated SON polynya area is an order of magnitude smaller than the total SIZ area, NPP within polynyas contributes ~17-23% of the total NPP during the December peak. These results highlight that polynya-like features are playing an important role in Antarctic marine productivity in the CESM2.



555 **Figure 7. JRA-CESM 1979-2020 climatological integrated SH monthly total NPP (top) and area-averaged NPP (bottom) for the sea ice zone (SIZ: blue) and SON polynya regions identified using 0.4 SIT (green) and 85% SIC (orange) thresholds.**

5 Discussion

Polynyas are often qualitatively defined -- “open water surrounded by ice and/or ice and land” -- and a leading conclusion of this work is that care must be taken when identifying quantitative polynya data from gridded products. Polynyas are a feature of the sea icescape – a complex, dynamically changing structure that is an integrated component of polar marine ecosystems as well as a leading player in polar oceanic and atmospheric circulations and dynamics.

560

Ideal metrics and thresholds for polynya identification will depend on the product grid sizes, region of interest, season and scientific application, as well as the specifications of an individual data product. Many coastal polynyas occur on smaller scales than can be resolved by the original EASE grids of the satellite based SIC products much less the typical nominal 1° grid of ESMS. An important result of this work is that although grid size may preclude resolving many individual polynyas (particularly many coastal polynyas), “polynya-like features“ may indeed be identified.

Gridded SICs retrieved from satellite images reveal much about the sea icescape, yet different retrieval algorithms can result in extremely small differences in hemispheric and regional integrated sea ice extents and areas, and simultaneously significant differences in temporal variability, correlations and trends in sub-grid scale features, as shown in this analysis of polynyas identified using SIC thresholds. These differences may be partially due to the difficulty of capturing areas of low SICs and/or low SITs through remote sensing, although disentangling the sources of these discrepancies is beyond the scope of this work. That the same passive microwave data but different retrieval algorithms can lead to uncorrelated timeseries of SH polynya areas and numbers once the data have been regridded and averaged monthly is remarkable. Polynya areas identified in both observational products are, however, significantly correlated spatially (longitudinally), regardless of spatial (EASE vs model) and temporal grids (daily vs monthly). This result suggests that on a climatological scale, locations of polynya-like features identified in both observation products are consistent even if their temporal variability, correlations and trends are not. Spatial cross-correlations between polynya features identified in the JRA-CESM output are significant, albeit lower than between the two observational products. The CESM2, like many ESMS, does not simulate land fast ice and therefore landfast ice cannot serve as anchors for coastal polynyas in the model which may contribute to this discrepancy.

Inconsistencies between identified polynyas in these two observational products complicate comparisons with ESM output, which are typically on coarser grids and daily or monthly averages rather than daily snapshots. Polynya features identified within both observational products and the JRA-CESM are consistent in terms of climatological means and geographic locations, even as temporal correlations, variabilities and trends are inconsistent between all the products (when on the same grid). The highest spatial (longitudinal) cross-correlations between the JRA-CESM and NOAA polynyas are nearly as large as cross-correlations between the two observational products (after regridding). The JRA-CESM successfully simulates polynya-like features in the icescape along the Antarctic coast, in a manner that is spatially consistent with both the NOAA and the OSISAF products, although the JRA-CESM tends to simulate lower polynya areas in the Bellingshausen-Amundsen sea than those estimated from the either product. Polynya-like features identified in the JRA-CESM show significantly higher NPP in these features identified using both SIT and SIC thresholds, than in the sea ice zone as a whole, and thus this method of identifying polynya-like regions successfully identifies biological hotspots in the model: NPP within polynyas in the JRA-CESM contributes to about 18% of the total Antarctic SH marine NPP even though the sea ice zone is roughly ten times as large as the springtime coastal polynya areas.

We provide some “best practices” from this systematic comparison of polynya identification methods in satellite-based and the CESM below and discuss the implications of polynya metric choices for applications in climate models.

5.1 Polynya metric choices: Temporal and spatial resolutions

600 Analysis of polynyas identified in both satellite and model products suggest that integrated SH climatologies made from daily vs monthly data do not differ significantly, and thus monthly data may be sufficient for some analyses on longer temporal scales. Integrated polynya (area and number) timeseries self- and cross-correlations are reduced when regriding the observational SIC data, to the point that regrided (from EASE to model grids) monthly data from the two observational products are not significantly correlated – yet the spatial cross-correlations remain significant even after regriding between 605 the two products. Thus, the method used here identifies polynya-like features that are geographically consistent between the two regrided observational products and yet inconsistent in temporal variability. We therefore recommend that in order to eliminate discrepancies due to grid types and resolutions alone, we recommend comparing metrics from data on the same grids (temporal and spatial), and regriding - if necessary - data with the higher geographical resolution onto the coarser resolution grid. Trends in polynya areas are not robust – including in significance, magnitude and sign – across the range of SIC 610 thresholds, grids and product sources (retrieval algorithms) in the observations analysed here. These inconsistencies between temporal variabilities, cross-correlations, and trends, and consistencies in geographical cross-correlations between polynyas in the two observational products suggest that the observational products may serve as good (poor) sources of verification of polynyas in ESM data spatially (temporally).

5.2 Polynya product and metric choice in modelled data

615 Using SICs, in general, to identify SH wintertime coastal polynyas in model simulations requires very high thresholds and is particularly problematic in the Bellingshausen-Amundsen Sea. Part of this issue is likely because ocean surface waters can very rapidly refreeze and form very high sea ice concentrations in all models, not just the CESM. Degrading model output to more closely resemble satellite estimates of SICs leads to only small increases in polynya areas identified using SICs (at 85% threshold) and does not explain the large bias between polynyas identified in winter (JJA) in both observational products and 620 the JRA-CESM. We thus find that identification of wintertime polynyas in the CESM better reproduces observed polynyas when using a SIT-based threshold, which more accurately accounts for low sea ice areas than SICs, which can be very high in the model even in very thin sea ice conditions, unlike in satellite imagery. We anticipate that other models will also have large discrepancies in wintertime coastal polynyas identified using SIT vs SIC and suggest considering a SIT-based metric for winter-time coastal polynya identification from model output.

625

It is interesting to note that while significant longitudinal correlations exist between polynya features identified in the JRA-CESM and the OBS for each month of the year and annually (Fig. 4c), the same cannot be said for temporal correlations of the integrated time series (Figs. 5c and 6a-e). This suggests that the regionality of the identified polynyas in the JRA-CESM is

captured well compared to the observations, however the temporal variability is less well captured in some regions and seasons. Part of this may be explained by the reanalysis data used to force the JRA-CESM and the nature of coastal polynyas. Reanalysis wind products show the lowest biases compared with weather station data in regions and times of high synoptic and/or low katabatic wind activity, and significant biases in wind fields close to the coast near where katabatic winds significantly impact coastal winds (e.g. Jones et al., 2016; Harrison et al., 2022). Katabatic winds are integral to the formation of coastal polynyas (e.g. Thompson et al., 2020 and references therein). Thus, coastal polynya variability due to variability in katabatic winds may be captured by the polynya time series in the observations but not well represented in the atmospheric reanalysis data used to force the model.

Recent work found significant positive trends in annual polynya areas in the Ross, Weddell, Indian and Pacific sectors estimated using daily data from the OSISAF CDR product at a 50% threshold on the 25 km x 25 km EASE grid (Duffy et al., 2023). Our results show significant positive polynya area trends in the OSISAF on the EASE grid only in the Indian sector (JJA and SON) and integrated across the SH (JJA) with a 50% SIC threshold. These contradictions may be due to differences in metrics or methods used to identify polynyas - an analysis beyond the scope of this work - yet it highlights that caution should be taken when comparing results from different sources, grids, methods and metrics. Indeed, one of our primary conclusions from this work is that trends of polynya-like features identified on grids that may not truly resolve distinct polynyas (as opposed to polynya-like features) should be viewed with caution, as different thresholds may result in even different signs of significant trends.

5.3 Polynya applications: coastal polynyas and NPP in a changing climate

Our analysis with the JRA-CESM demonstrates that the CESM is indeed capturing enhanced productivity within polynya-like features in austral spring compared to within the entire SIC. Elevated rates of NPP occur in polynya features identified using either a 0.4 m SIT or an 85% SIC thresholds, with similar rates of productivity in SIC and SIT-defined polynyas. NPP within these polynya-like features contributes ~17-23% of the total sea ice zone NPP during the December peak, even though the area of these polynyas is only ~3% of the sea ice zone. This finding underscores how critical polynyas are for the base of the Antarctic food web, and using models to understand these areas is particularly critical given the challenges of satellite chlorophyll retrievals in these areas (e.g. Oliver et al. 2025).

6 Conclusions

The definition of “polynyas” in a quantifiable sense is relatively subjective. Defining areas and timing of open water within the Antarctic sea ice zone such that comparisons can be made between satellite based SICs and model output requires careful consideration and recognition of the basic differences between satellite observations and model output as well as considerations of grid size, metric and threshold. Coastal polynyas exist often at spatial scales smaller than the grid scales from both

660 observational and simulated data. As such, polynya metrics may not resolve polynyas per se, but rather grid cells that contain polynya-like features. One of the most surprising results of this work is the astonishing inconsistencies between polynya area time series variabilities and trends due that result using different retrieval algorithms and/or regridding. Temporal trends show particularly large inconsistencies – including in sign – across algorithm, grid, and threshold. These inconsistencies in temporal variabilities and trends of sub-grid scale icescape features such as polynyas suggest that temporal characteristics such as
665 variability and trends may not be adequately captured by this method of identifying polynya-like features on gridded data, whether in observationally based products or model output. On the other hand, polynya-like features are consistent spatially across both observationally based products and the hindcast model output.

Our conclusions with respect to our primary four questions are:

- 670 1. The JRA-CESM captures climatologically and biologically relevant coastal polynya-like features and coastal winter polynyas identified using sea ice thicknesses in model data are more consistent with wintertime polynyas identified in satellite-based products.
- 675 2. Temporal variabilities and trends are inconsistent not only between polynya-like features in the model and the observational products, but also between the two observational products, grid and threshold.
3. Spatial locations of winter-spring coastal polynya-like features are consistent between both NOAA and OSISAF, as well as between the JRA-CESM and both observational products.
- 680 4. Coastal polynya-like features in the JRA-CESM serve as biological hotspots, contributing ~17-23% of the total sea ice zone marine net primary productivity even while occupying only about 3% of the area of the sea ice zone, consistent with observational studies.

Appendices

Appendix A: Polynya algorithm

685 The polynya algorithm cycles through maps of the sea ice variable (concentration or thickness in this work) and initially labels any grid cells that fall below the threshold and that lie within the sea ice zone (south of the open ocean boundary). The algorithm iteratively cycles through the polynya maps to determine if grid cells that meet the threshold criteria are surrounded by sea ice and land (in which case they are labelled a polynya) or lie next to open ocean (in which case they are not identified as a polynya). Figure AA1 shows a schematic of a hypothetical region with land, ocean, sea ice and polynya grid cells. In this
690 example, there are two polynyas – one open water polynya (occupied by three grid cells), and one coastal polynya (occupied

by two grid cells). Figure AA2 shows an example satellite image of the Ross Bay and Terra Nova polynyas and grid cells labelled by SICs.

695

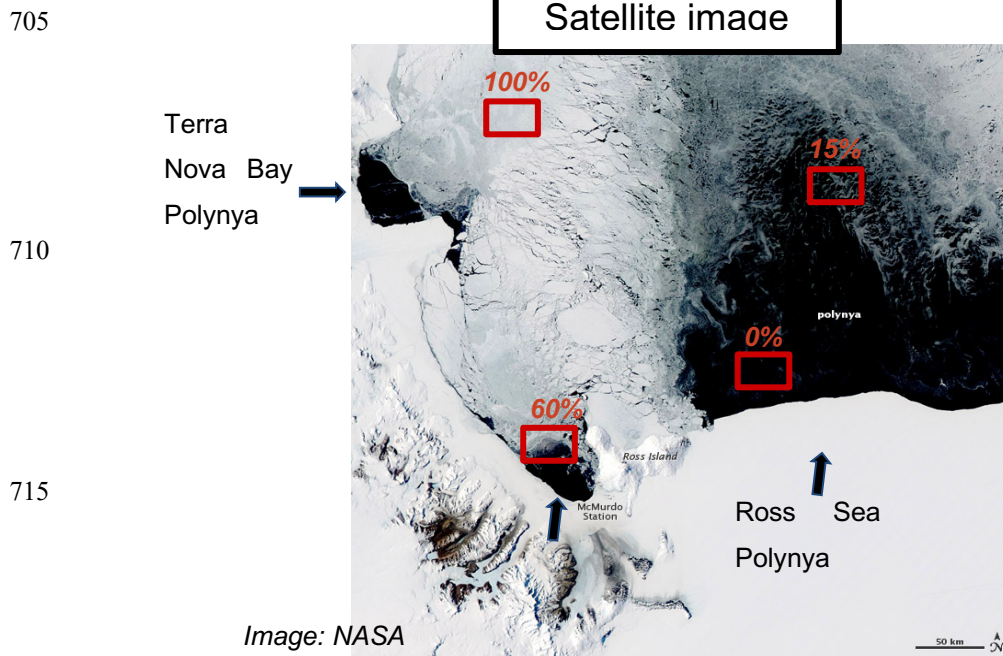
No	No				
No	No		OWP		
		OWP	OWP		CP
					CP

No = not polynya
OWP = open water polynya
CP = coastal polynya

	0% SIC (open ocean)
	< threshold (e.g. 50% SIC)
	> threshold (e.g. 90% SIC)
	Land

700

Figure A1. Schematic of grid cells considered open ocean (dark blue), land (light green) and within the sea ice zone (light and medium blue). Grid cells in the sea ice zone that meet the threshold criteria are in medium blue; grid cells that lie above the threshold are in light blue. Grid cells that meet the criteria are identified as polynyas only if they are bounded by sea ice (open water polynyas) or sea ice and land (coastal polynyas).



720 **Figure A2.** Example satellite image of the Terra Nova Bay and Ross Sea polynyas (Moderate Resolution Imaging Spectroradiometer (MODIS) image of the day from the National Aeronautics and Space Administration (NASA) Aqua satellite, November 16, 2011 https://eoimages.gsfc.nasa.gov/images/imagerecords/76000/76474/rosssea_amo_2011320_lrg.jpg). Hypothetical grid cells with SICs are shown in red.

Appendix B: Grid size and type and impact on polynya identification

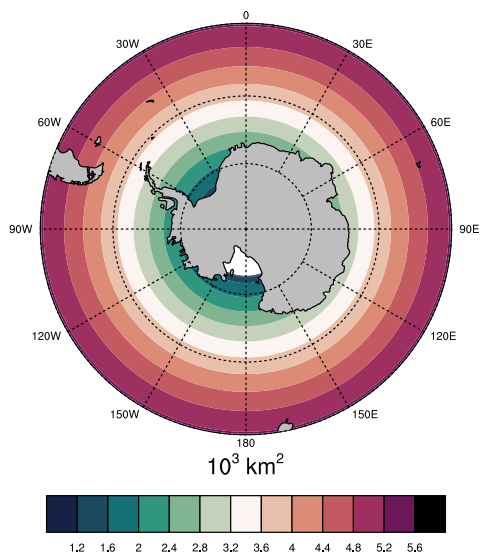
Using concentration thresholds to define polynya regions will define how much open water (and likewise sea ice) is in the grid cell by percentage. For an Equal Area Scaleable Earth (EASE) grid this will correspond to an area that doesn't change with latitude or longitude, whereas on an equal latitude-longitude grid a SIC percent threshold will correspond to different areas of open water (or sea ice) depending on latitude. For example, a 50% sea ice concentration threshold on a 25kmx25km EASE grid corresponds to 312.5 km² or more of open water (and also 312.5 km² of sea ice) within the grid cell to meet the threshold requirement for a polynya. A grid based on latitude and longitude, which is common for earth system models, will have a varying range of surface area in each grid cell. A grid cell of $\sim 3.2 \cdot 10^3$ km² (about the area of grid cells next to the Antarctic coast on the Pacific and Indian sectors in the CESM) would have 312.5 km² of open water at a SIC threshold of 90%. Figure AB1 shows the area of the grid cells in the ocean grid in the CESM2 and areas of open water that would be contained in grid cells for example SIC thresholds. An example of the SIC thresholds required to result in 312.5 km² of open water within a grid are shown in Fig. AB2 for an equal area grid cell and two grid cells from a 1°x1° grid cell at two different latitudes. Different grids can also lead to different areas and numbers of polynyas even when the open water areas are the same (e.g. Fig. AB3).

725

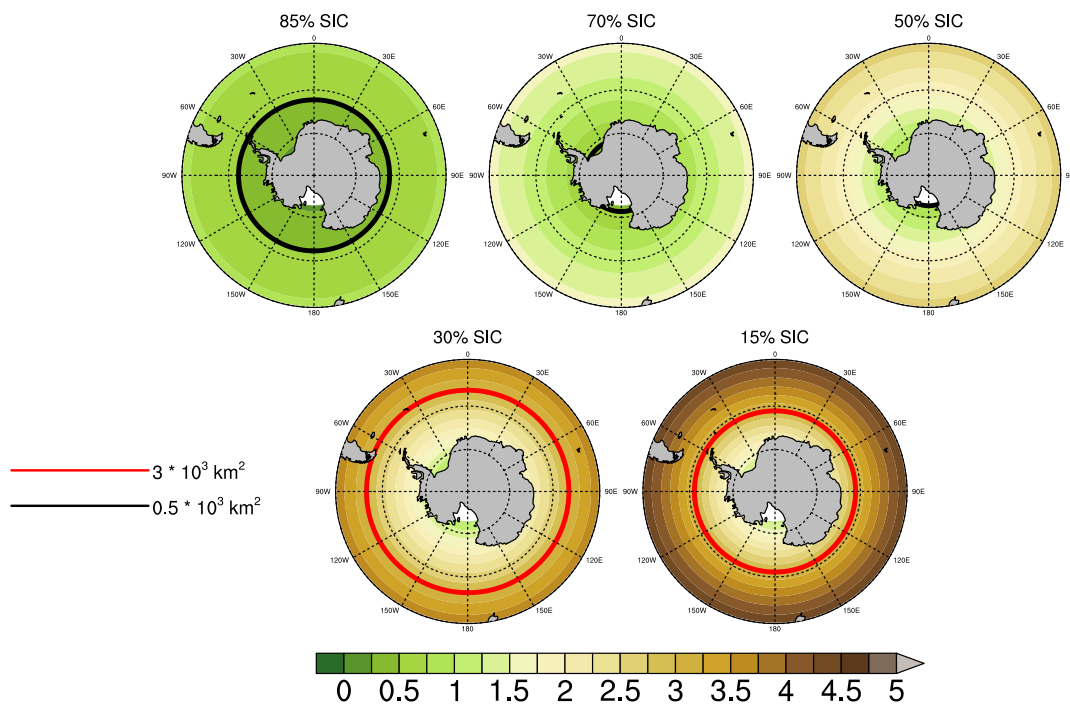
730

735

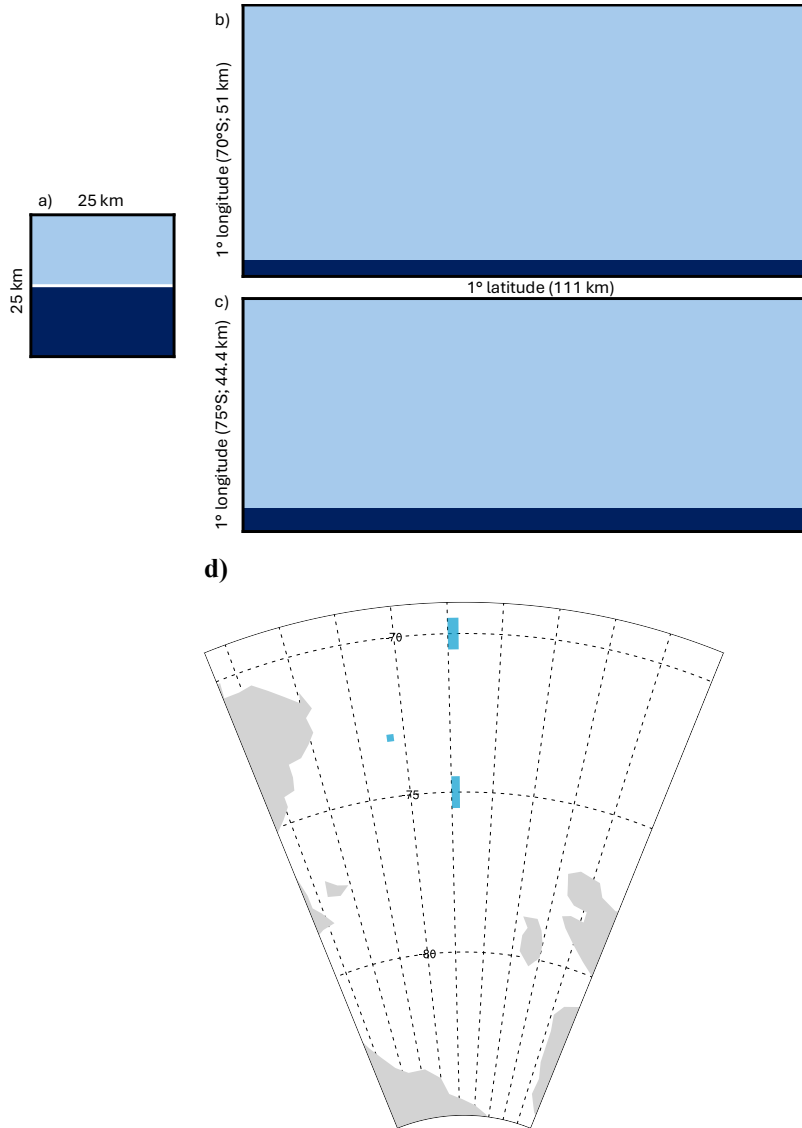
CESM2 grid cell area



Total area of open water in grid cell for given SIC (10^3 km^2)



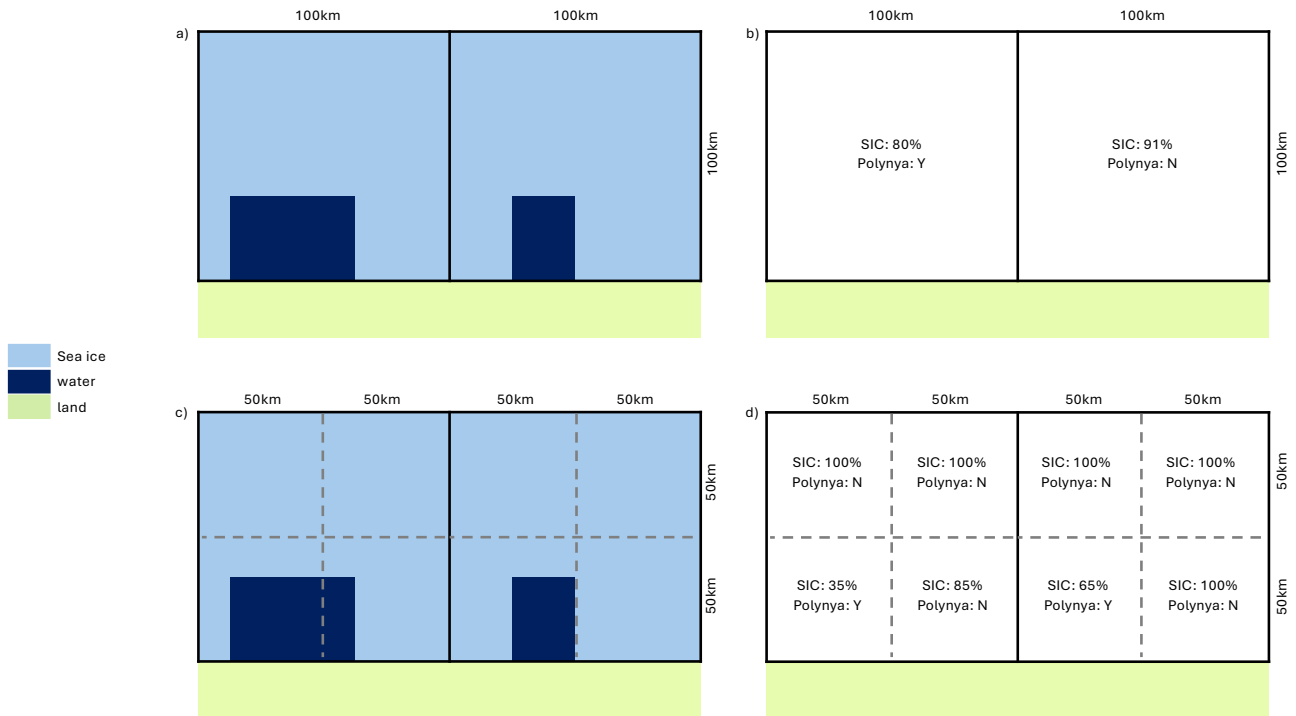
740 **Figure B1.** Area of the ocean grid cells in the CESM2 ($\times 10^3 \text{ km}^2$; top) and total area ($\times 10^3 \text{ km}^2$) of open water for a given SIC threshold in the CESM2 grid (bottom). Red/black contours indicate $3 \times 10^3 \text{ km}^2$ / $0.5 \times 10^3 \text{ km}^2$ of open water, respectively.



745

750

Figure B2. Sea ice concentration required to result in 312.5 km² of open water within a grid cell: a) SIC 50% on a 25 km x 25 km equal area grid cell, b) 94.8% SIC on a 1°x1° lat/lon grid cell at 70°S (approximately 111km x 51km), and c) 93.7% SIC on a 1°x1° lat/lon grid cell at 75°S (approximately 111km x 44.4km). Panel d shows the area occupied by grid cells (in blue) in a, b, c in the Ross Sea as an illustration. Panels a-c are shown as rectangles for illustration even though 1° lat/lon grid cells are not exactly rectangular.



755 **Figure B3. Examples of grid cells classified as polynyas using an 80% SIC threshold on a larger resolution grid (a-b) and a smaller resolution grid (c-d). Coloured panels (a, c) indicate areas of ice (light blue), water (navy) and land (light green). Text in panels b, d indicate SIC for the grid cell and whether or not it would be identified as a polynya using an 80% SIC threshold. The top example has one polynya grid cell and double the integrated polynya area (10000 km²) over the entire region compared to the second example (2 grid cells and 5000 km²).**

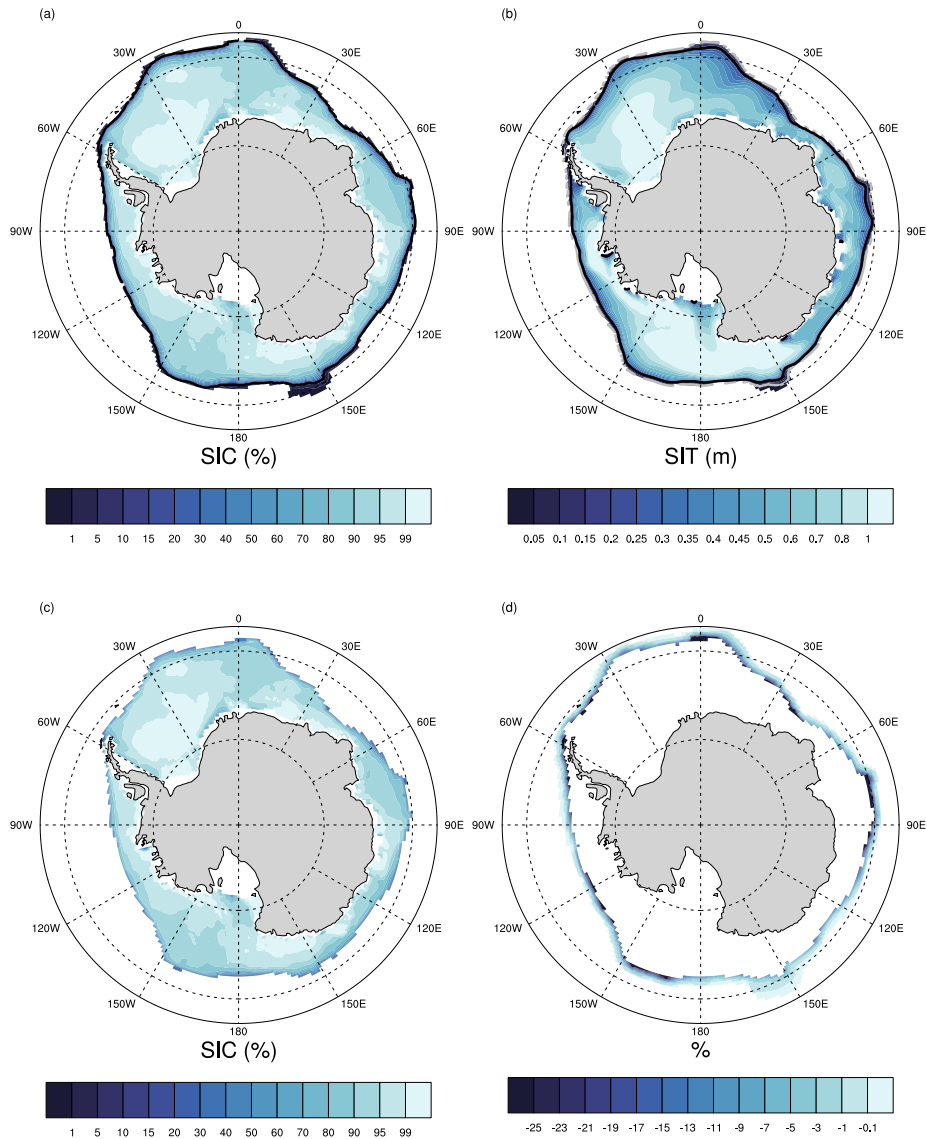
760

Appendix C: Degrading climate model daily SIC data.

Figure AC1 shows an example of model SICs that are degraded such that the new sea ice concentrations are set to 0 where the original SICs are less than 10% and where SITs are less than 5 cm. In regions of SITs that fall between 5cm and 20 cm, SICs are set to half of the original values. The resulting degraded product has noticeably lower SICs along the ice perimeter and

765 isolated locations near the Antarctic continent with lower SICs.

JRA_4p2z
JUL 15 2003



770 **Figure C1.** Sea Ice Concentration (a) and sea ice thickness (b) from the JRA-CESM run on July 15, 2003. Degraded sea ice (c) and (d) the resulting change in SIC by degrading the sea ice.

Code and data availability

The CESM2-LE data used in this study are freely available, as described in Rodgers et al. (2021). The JRA hindcast simulations (Forced Ocean Sea Ice, FOSI) are freely available from the Earth System Grid (<https://app.globus.org/file->

775 manager?origin_id=6b1c030c-af71-4336-b083-8c179f843567&origin_path=%2F&two_pane=false). Scripts for identifying polynya-like features, analysing polynyas and making the figures in this manuscript are available in a public repository: https://github.com/lldrum/Cryosphere_AntarcticPolynyas_SatelliteModels_ecosystems. All observational datasets used for model validation are publicly available.

Author contributions

780 Study design and analysis were conducted by LL with ideas from MMH, AKD, KK and ZS. All authors contributed to the writing of the manuscript.

Competing Interests

The authors declare that they have no conflict of interest.

Acknowledgements

785 The National Science Foundation (NSF) National Center for Atmospheric Research (NCAR) is sponsored by NSF under cooperative agreement no. 1852977. Previous and current CESM versions are freely available online (at <https://www.cesm.ucar.edu/models/cesm2/>). The CESM data sets used in this study are freely available online from the NCAR Digital Asset Services Hub (at <https://doi.org/10.5065/bgt9-tz46>). We thank all the scientists, software engineers, and administrators who contributed to the development and availability of CESM. The CESM project has been supported primarily
790 by the National Science Foundation. We would like to acknowledge high-performance computing support from the Derecho system ([doi:10.5065/qx9a-pg09](https://doi.org/10.5065/qx9a-pg09)) provided by the Computational and Information Systems Laboratory at NSF NCAR.

We acknowledge support for this work from National Aeronautics and Space Administration (NASA) and the National Science Foundation (NSF) as detailed below. Any opinions, findings, and conclusions or recommendations expressed in this material
795 are those of the authors and do not necessarily reflect the views of these agencies. LL, MMH and KK acknowledge support for this work from the NASA Award 80NSSC20K1289 and the NSF Award 2037531. LL, AKD, KK and ZS acknowledge support for this work from the NASA Award 80NSSC21K1132.

This study has been conducted using OSI SAF Global sea ice concentration climate data record 1978-2020 (v3.0, 2022), OSI-
800 450-a, doi:10.15770/EUM_SAF_OSI_0013. EUMETSAT Ocean and Sea Ice Satellite Application Facility. Data extracted from E. U. Copernicus Marine Service Information: accessed 23 January, 2025.

References

- Arrigo, K. R., and G. L. van Dijken: Phytoplankton dynamics within 37 Antarctic coastal polynyas, *J. Geophys. Res.*, 108(C8), 3271, doi:[10.1029/2002JC001739](https://doi.org/10.1029/2002JC001739), 2003.
- 805 Arrigo, K. R., G. L. van Dijken, and A. L. Strong: Environmental controls of marine productivity hot spots around Antarctica, *J. Geophys. Res. Oceans*, 120, 5545–5565, doi:[10.1002/2015JC010888](https://doi.org/10.1002/2015JC010888), 2015.
- Comiso, J. C.: Characteristics of arctic winter sea ice from satellite multispectral microwave observations, *J. Geophys. Res.*, 91, 975–994, 1986.
- Bocquet, M., S. Fleury, F. Rémy, and F. Piras, F.: Arctic and Antarctic sea ice thickness and volume changes from
810 observations between 1994 and 2023. *Journal of Geophysical Research: Oceans*, 129, e2023JC020848. <https://doi.org/10.1029/2023JC020848>, 2024.
- Cavalieri, D. J., P. Gloersen, and W. J. Campbell: Determination of sea ice parameters with the NIMBUS 7 SMMR, *J. Geophys. Res.*, 89, 5355–5369, 1984.
- Comiso, J. C., D. Cavalieri, C. Parkinson C., and P. Gloersen: Passive microwave algorithms for sea ice concentrations: a
815 comparison of two techniques. *Remote Sensing of the Environment*, 60, 357–384, 1997.
- Criscitiello, A. S., S. B. Das, M. J. Evans, K. E. Frey, H. Conway, I. Joughin, B. Medley, and E. J. Steig: Ice sheet record of recent sea-ice behavior and polynya variability in the Amundsen Sea, West Antarctica, *J. Geophys. Res. Oceans*, 118, 118–130, doi:[10.1029/2012JC008077](https://doi.org/10.1029/2012JC008077), 2013.
- Danabasoglu, G., J. F. Lamarque, J. Bacmeister, D. Bailey, A. K. DuVivier, J. Edwards, et al.: The Community Earth System
820 Model version 2 (CESM2). *J. Adv. in Model. Earth Sys.*, 2, 1–35. <https://doi.org/10.1029/2019ms001916>, 2020.
- Duffy, G. A., F. Montiel, A. Purich, and C. I. Fraser: Emerging long-term trends and interdecadal cycles in Antarctic polynyas, *Proc. of the Nat. Acad. of Sci.*, 121 (11), <https://doi.org/10.1073/pnas.2321595121>, 2024.
- Diamond, R., L. C. Sime, C. R. Holmes, and D. Schroeder: CMIP6 models rarely simulate Antarctic winter sea-ice anomalies as large as observed in 2023. *Geophysical Research Letters*, **51**(10),
825 e2024GL109265. <https://doi.org/10.1029/2024GL109265>, 2024.
- DuVivier, A. K., M. M. Holland, L. Landrum, H. A. Singh, D. A. Bailey, and E. A. Maroon: Impacts of sea ice mushy thermodynamics in the Antarctic on the coupled Earth system, *Geophys. Res. Lett.*, 48, e2021GL094287, <https://doi.org/10.1029/2021GL094287>, 2021.
- DuVivier, A. K., M. J. Molina, A. L. Deppenmeier, M. M. Holland, L. Landrum, K. Krumhardt, & S. Jenouvrier. Projections
830 of winter polynyas and their biophysical impacts in the Ross Sea Antarctica. *Clim Dyn.* 2024;62(2):989-1012. doi: 10.1007/s00382-023-06951-z. Epub 2023 Sep 23. PMID: 39328888; PMCID: PMC11424701, 2024.
- Eyring, V., S. Bony, G. A. Meehl, C. A. Senior, B. Stevens, R. J. Stouffer, and K. E. Taylor: Overview of the Coupled Model Intercomparison Project Phase 6 (CMIP6) experimental design and organization. *Geosc. Model Devel.*, 9(5), 1937–1958, <https://doi.org/10.5194/gmd-9-1937-2016>, 2016.

- 835 Fetterer, F., K. Knowles, W. N. Meier, M. Savoie, and A. K. Windnagel: Sea Ice Index, Version 3. Distributed by National Snow and Ice Data Center, Boulder, Colorado, USA (accessed 2 June 2023); <https://doi.org/10.7265/N5K072F8>, 2017.
- Flores, H., G. Veyssière, G. Castellani, *et al.*: Sea-ice decline could keep zooplankton deeper for longer. *Nat. Clim. Chang.* 13, 1122–1130, <https://doi.org/10.1038/s41558-023-01779-1>, 2023.
- Fogt, R. L., A. M. Sleinkofer, M. N. Raphael, *et al.*: A regime shift in seasonal total Antarctic sea ice extent in the twentieth century. *Nat. Clim. Chang.* 12, 54–62, <https://doi.org/10.1038/s41558-021-01254-9>, 2022.
- 840 Fons, S., Kurtz, N., and Bagnardi, M.: A decade-plus of Antarctic sea ice thickness and volume estimates from CryoSat-2 using a physical model and waveform fitting, *The Cryosphere*, 17, 2487–2508, <https://doi.org/10.5194/tc-17-2487-2023>, 2023.
- Fraser, A. D., K. I. Ohshima, S. Nihashi, R. A. Massom, T. Tamura, K. Nakata, G. D. Williams, S. Carpentier, and S. Willmes: Landfast ice controls on sea-ice production in the Cape Darnley Polynya: A case study, *Remote Sensing of Environment*, Volume 233, 111315, ISSN 0034-4257, <https://doi.org/10.1016/j.rse.2019.111315>, 2019.
- 845 Gilbert, R. O.: *Statistical Methods for Environmental Pollution Monitoring*, Wiley, NY, 1987.
- Harrison, T. C., S. Biri, T. J. Bracegirdle, J. C. King, E. C. Kent, E. Vignon, and J. Turner, J.: Reanalysis representation of low-level winds in the Antarctic near-coastal region, *Weather Clim. Dynam.*, 3, 1415–1437, <https://doi.org/10.5194/wcd-3-1415-2022>, 2022.
- 850 Grenfell, T. C., D. J. Cavalieri, J. C. Comiso, M. R. Drinkwater, R. G. Onstott, I. Rubinstein, K. Steffen, and D. P. Winebrenner: Considerations for microwave remote sensing of thin sea ice, in: *Microwave Remote Sensing of Sea Ice*, edited by: Carsey, F. D., American Geophysical Union, Washington, D.C., doi:10.1029/GM068p0291, 1992.
- Holmes, C. R., T. J. Bracegirdle, P. R. Holland, J. Stroeve, and J. Wilkinson: Brief communication: New perspectives on the skill of modelled sea ice trends in light of recent Antarctic sea ice loss, *The Cryosphere*, 18, 5641–5652, <https://doi.org/10.5194/tc-18-5641-2024>, 2024.
- 855 Hobbs, W., and Coauthors: Observational Evidence for a Regime Shift in Summer Antarctic Sea Ice. *J. Climate*, 37, 2263–2275, <https://doi.org/10.1175/JCLI-D-23-0479.1>, 2024.
- Holland, M. M., C. M. Bitz, E. C. Hunke, W. H. Lipscomb, and J. L. Schramm: Influence of the sea ice thickness distribution on polar climate in CCSM3. *Journal of Climate*, 19(11), 2398–2414. <https://doi.org/10.1175/jcli3751.1>, 2006.
- 860 Hunke, E. C., W. H. Lipscomb, A. K. Turner, N. Jeffery, and S. Elliott: CICE: The Los Alamos Sea Ice Model. Documentation and software user's manual. Version 5.1. T-3 Fluid Dynamics Group, Los Alamos National Laboratory, Tech. Rep. LA-CC-06-012, 2015.
- Ivanova, N., L. T. Pedersen, R. T. Tonboe, S. Kern, G. Heygster, T. Lavergne, A. Sorensen, R., Saldo, G. Dybjaer, L. Brucker, and M. Shokr: Inter-comparison and evaluation of sea ice algorithms: towards further identification of challenges and optimal approach using passive microwave observations, *The Cryo.*, 9, 1797-1817, <https://doi.org/10.5194/tc-9-1797-2015>, 2015.
- 865 Jeong, H., S. S. Lee, H. S. Park, *et al.*: Future changes in Antarctic coastal polynyas and bottom water formation simulated by a high-resolution coupled model. *Commun Earth Environ* 4, 490. <https://doi.org/10.1038/s43247-023-01156-y>, 2023.

- Jones, R., I. Renfrew, A. Orr, B. Webber, D. Holland, and M. Lazzara: Evaluation of four global reanalysis products using in situ observations in the Amundsen Sea Embayment, Antarctica, *J. Geophys. Res.-Atmos.*, 121, 6240–6257, 2016.
- 870 Kacimi, S., and R. Kwok: Arctic snow depth, ice thickness, and volume from ICESat-2 and CryoSat-2: 2018–2021. *Geophys. Res. Letts.*, 49, e2021GL097448. <https://doi.org/10.1029/2021GL097448>, 2022.
- Kendall, M.G.: *Rank Correlation Methods*, 4th edition, Charles Griffin, London, 1975.
- Kern, S., G. Spreen, L. Kaleschke, S. De La Rosa, and G. Heygster: Polynya Signature Simulation Method polynya area in comparison to AMSR-E 89GHz sea-ice concentrations in the Ross Sea and off the Adélie Coast, Antarctica, for 2002–05: first
875 results, *Ann. Glaciol.*, 46, 409–418, 2007.
- Kobayashi, S., O. T. A. Yukinari, Y. Harada, A. Ebita, M. Moriya, H. Onoda, K. Onogi, H. Kamahori, C. Kobayashi, K. Miyaoka, and K. Takahashi: The JRA-55 reanalysis: general specifications and basic characteristics. *J Meteorol Soc Jpn Ser II* 93(1), 5–48, <https://doi.org/10.2151/jmsj.2015-001>, 2015.
- Krumhardt K. M., M. C. Long, A. T. Sylvester, and C. M. Petrik: Climate drivers of Southern Ocean phytoplankton community
880 composition and potential impacts on higher trophic levels. *Front. Mar. Sci.* 9:916140. doi: 10.3389/fmars.2022.916140, 2022.
- Krumhardt, K. M., M. C. Long, C. M. Petrik, M. Levy, F. S. Castruccio, K. Lindsay, L. Romashkov, A.-L. Deppenmeier, R. Denéchère, Z. Chen, L. Landrum, G. Danabasoglu, and P. Chang: From nutrients to fish: Impacts of mesoscale processes in a global CESM-FEISTY eddying ocean model framework, *Prog. in Ocean.*, 227, 2024, 103314, ISSN 0079-6611, <https://doi.org/10.1016/j.poccean.2024.103314>, 2024.
- 885 Kwok, R., J. C. Comiso, S. Martin, and R. Drucker: Ross Sea polynyas: Response of ice concentration retrievals to large areas of thin ice, *J. Geophys. Res.*, 112, C12012, doi:10.1029/2006JC003967, 2007.
- Labrousse, S., A. D. Fraser, M. Sumner, T. Tamura, D. Pinaud, B. Wienecke, et al.: Dynamic fine-scale sea icescape shapes adult emperor penguin foraging habitat in East Antarctica. *Geophys. Res. Lett.* 46, 11206–11218. doi: 10.1029/2019GL084347, 2019.
- 890 Lavergne, T., A. M. Sørensen, S. Kern, R. Tonboe, D. Notz, S. Aaboe, L. Bell, G. Dybkjær, S. Eastwood, C. Gabarro, G. Heygster, M. A. Killie, M. Brandt Kreiner, J. Lavelle, R. Saldo, S. Sandven, and L. T. Pedersen: Version 2 of the EUMETSAT OSI SAF and ESA CCI sea-ice concentration climate data records, *The Cryo.*, 13, 49–78, <https://doi.org/10.5194/tc-13-49-2019>, 2019.
- Li, Y., R. Ji, S. Jenouvrier, M. Jin, and J. Stroeve: Synchronicity between ice retreat and phytoplankton bloom in circum-
895 Antarctic polynyas, *Geophys. Res. Lett.*, 43, 2086–2093, doi:10.1002/2016GL067937, 2016.
- Mann, H.B.: Non-parametric tests against trend, *Econometrica* 13:163-171, 2045.
- Markus, T. and B. A. Burns: Detection of coastal polynyas with passive microwave data. *Ann. Glaciol.*, 17, 351- 355, 1993.
- Massom, R. A., P. T. Harris, K. J. Michael, and M. J. Potter: The distribution and formative processes of latent-heat polynyas in East Antarctica, *Ann. Glaciol.*, 27, 420– 426, 1998.
- 900 Meier, W.N.: Comparison of passive microwave ice concentration algorithm retrievals with AVHRR imagery in Arctic peripheral seas. *IEEE Trans. Geo. Remote Sensing*, 43, 1324-1337, 2005.

- Meier, W. N., G. Peng, D. J. Scott, and M. H. Savoie: Verification of a new NOAA/NSIDC passive microwave sea-ice concentration climate record. *Polar Research*, 33. doi: 10.3402/polar.v33.21004, 2014.
- Meier, W. N., F. Fetterer, A. K. Windnagel, and J. S. Stewart: *NOAA/NSIDC Climate Data Record of Passive Microwave Sea Ice Concentration, Version 4*. Southern Hemisphere, 1979-2020. Boulder, Colorado USA. NSIDC: National Snow and Ice Data Center. doi: <https://doi.org/10.7265/efmz-2t65>, 2021. Accessed June 3, 2023.
- Meier, W. N., A. Windnagel, and S. Stewart: CDR Climate Algorithm and Theoretical Basis Document: Sea Ice Concentration. NOAA NCEI CDR Program, 2021.
- Mohrmann, M., C. Heuzé, and S. Swart: Southern Ocean polynyas in CMIP6 models, *The Cryo.*, 15, 4281–4313, 910 <https://doi.org/10.5194/tc-15-4281-2021>, 2021.
- Nakata, K., K. I. Ohshima, S. Nihashi, N. Kimura, and T. Tamura: Variability and ice production budget in the Ross Ice Shelf Polynya based on a simplified polynya model and satellite observations, *J. of Geophys. Res.: Oceans*, 120, 6234–6252, 2015.
- Nakata, K., K. I. Ohshima, and S. Nihashi: Mapping of Active Frazil for Antarctic Coastal Polynyas, With an Estimation of Sea-Ice Production. *Geophys. Res. Lett.*, 48, e2020GL091353, 2021.
- 915 Nihashi, S. and K. J. Ohshima: Circumpolar Mapping of Antarctic Coastal Polynyas and Landfast Sea Ice: Relationship and Variability, *J. Clim*, 28, 3650-3670, DOI: 10.1175/JCLI-D-14-00369.1, 2015.
- Notz, D.: Sea-ice extent and its trend provide limited metrics of model performance. *Cryo.* 8, 229–243. (doi:10.5194/tc-8-229-2014), 2014.
- Notz, D.: How well must climate models agree with observations?, *Philosophical Transactions of the Royal Society of London* 920 A: Mathematical, Phys. and Engin. Sci., 373, <https://doi.org/10.1098/rsta.2014.0164>, 2015.
- Oliver, H., J. S. Turner, A. Castagna, H. Houskeeper, and H. Dierssen: High Antarctic coastal productivity in polynyas revealed by considering remote sensing ice-adjacency effects. *Limnol. Oceanogr. Lett.* <https://doi.org/10.1002/lol2.70043>, 2025.
- Ohshima, K., Y. Fukamachi, G. Williams, *et al.*: Antarctic Bottom Water production by intense sea-ice formation in the Cape Darnley polynya. *Nature Geosci* 6, 235–240. <https://doi.org/10.1038/ngeo1738>, 2013.
- 925 Ohshima, K. I., S. Nihashi, and K. Iwamoto, K.: Global view of sea-ice production in polynyas and its linkage to dense/bottom water formation, *Geoscience Letters*, 3, 13, 2016.
- O'Reilly, J. E., S. Maritorena, B. G. Mitchell, D. A. Siegel, K. L. Carder, S. A. Garver, M. Kahru, and C. McClain, C.: Ocean color chlorophyll algorithms for SeaWiFS, *J. Geophys. Res.*, 103, 24,937– 24,953, 1998.
- OSI SAF Global sea ice concentration climate data record 1978-2020 (v3.0, 2022), OSI-450-a, 930 doi:10.15770/EUM_SAF_OSI_0013. EUMETSAT Ocean and Sea Ice Satellite Application Facility. Data extracted from E. U. Copernicus Marine Service Information: accessed 23 January, 2025.
- Parkinson, C. L. and D. J. Cavalieri: Antarctic sea ice variability and trends, 1979–2010, *The Cryo.*, 6, 871–880, <https://doi.org/10.5194/tc-6-871-2012>, 2012.
- Parkinson, C., and D. Cavalieri: Antarctic sea ice variability and trends, 1979–2010. *The Cryosphere*, 6, 871–880, 2012.

- 935 Parkinson, C. L.: A 40-y record reveals gradual Antarctic sea ice increases followed by decreases at rates far exceeding the rates seen in the Arctic, *P. Natl. Acad. Sci. USA*, 116, 14414–14423, 2019.
- Purich, A., and E. W. Doddridge: Record low Antarctic sea ice coverage indicates a new sea ice state. *Commun Earth Environ* 4, 314. <https://doi.org/10.1038/s43247-023-00961-9>, 2023.
- Raphael, M.N., and M. S. Handcock: A new record minimum for Antarctic sea ice. *Nat Rev Earth Environ* 3, 215–216.
- 940 <https://doi.org/10.1038/s43017-022-00281-0>, 2022.
- Richert, I., P. Yager, J. Dinasquet, R., Logares, L. Riemann, A. Wendeberg, S. Bertilsson, and D. Scofield: Summer comes to the Southern Ocean: how phytoplankton shape bacterioplankton communities far into the deep dark sea. *Ecosphere*. 10. e02641. 10.1002/eecs2.2641, 2019.
- Raphael, M. N., T. J. Maierhofer, R. L. Fogt, W. R. Hobbs, and M. S. Handcock: A Twenty-First Century Structural Change
- 945 in Antarctica’s Sea Ice System. *Communications Earth & Environment* 6, no. 1 (February 21, 2025): 1–9. <https://doi.org/10.1038/s43247-025-02107-5>, 2025
- Roach, L. A., J. Dörr, C. R. Holmes, F. Massonnet, E. W. Blockley, D. Notz, et al.: Antarctic sea ice area in CMIP6. *Geophysical Research Letters*, 47, e2019GL086729. <https://doi.org/10.1029/2019GL086729>, 2020.
- Singh, H. K. A., L. Landrum, M. M. Holland, D. A. Bailey, and A. K. DuVivier: An overview of Antarctic sea ice in the
- 950 CESM2: analysis of the seasonal cycle, predictability, and atmosphere-ocean-ice interactions. *J Adv Model Earth Syst.*, 13, <https://doi.org/10.1029/2020MS002143>, 2020.
- Smith, R., P. Jones, B. Briegleb, F. Bryan, G. Danabasoglu, J. Dennis, et al. The Parallel Ocean Program (POP) reference manual, Ocean component of the Community Climate System Model (CCSM), LANL Tech. Report, LAUR-10-01853, 141 pp, 2010.
- 955 Smith, A., A. Jahn, and M. Wang: Seasonal transition dates can reveal biases in Arctic sea ice simulations, *The Cryosphere*, 14, 2977–2997, <https://doi.org/10.5194/tc-14-2977-2020>, 2020.
- Smith, A., A. Jahn, C. Burgard, and D. Notz: Improving model-satellite comparisons of sea ice melt onset with a satellite simulator, *The Cryosphere*, 16, 3235–3248, <https://doi.org/10.5194/tc-16-3235-2022>, 2022.
- Stammerjohn, S. E., D. G. Martinson, R. C. Smith, X. Yuan, and D. Rind: Trends in Antarctic annual sea ice retreat and
- 960 advance and their relation to El Niño–Southern Oscillation and Southern Annular Mode variability, *J. Geophys. Res.*, 113, C03S90, doi:10.1029/2007JC004269, 2008.
- Tamura, T., K. I. Ohshima, H. Enomoto, K. Tateyama, A. Muto, S. Ushio, and R. A. Massom: Estimation of thin sea-ice thickness from NOAA AVHRR data in a polynya off the Wilkes Land coast, East Antarctica. *Ann. Glaciol.*, 44, 269–274, 2006.
- 965 Tamura, T., K. I. Ohshima, T. Markus, D. J. Cavalieri, S. Nishashi, and N. Hirasawa: Estimation of thin ice thickness and detection of fast ice from SSM/I data in the Antarctic Ocean, *J. Atmos. Oceanic Technol.*, 24, 1757– 1772, 2007.
- Tamura, T., K. I. Ohshima, and S. Nishashi: Mapping of sea ice production for Antarctic coastal polynyas. *Geophys Res Lett* 35:L07606, 2008.

- Tamura, T., K. I. Ohshima, A. D. Fraser, and G. D. Williams: Sea ice production variability in Antarctic coastal polynyas, *J. Geophys. Res. Oceans*, 121, 2967–2979, doi:10.1002/2015JC011537, 2016.
- Thompson, L., M. Smith, J. Thomson, S. Stammerjohn, S. Ackley, and B. Loose: Frazil ice growth and production during katabatic wind events in the Ross Sea, Antarctica, *The Cryosphere*, 14, 3329–3347, <https://doi.org/10.5194/tc-14-3329-2020>, 2020.
- Tsujino, H., S. Urakawa, H. Nakano, R. J. Small, W. M. Kim, S. G. Yeager, G. Danabasoglu, T. Suzuki, J. L. Bamber, M. Bentsen, C. W. Böning, A. Bozec, E. P. Chassignet, E. Curchitser, F. Boeira Dias, P. J. Durack, S. M. Griffies, Y. Harada, M. Ilicak, S. A. Josey, C. Kobayashi, S. Kobayashi, Y. Komuro, W. G. Large, J. Le Sommer, S. J. Marsland, S. Masina, M. Scheinert, H. Tomita, M. Valdivieso, and D. Yamazaki: Jra-55 based surface dataset for driving ocean–sea-ice models (jra55-do). *Ocean Modelling*, **130**:79–139, 2018.
- Turner, J., T. Phillips, G. J. Marshall, J. S. Hosking, J. O. Pope, T. J. Bracegirdle, and P. Deb: Unprecedented springtime retreat of Antarctic sea ice in 2016, *Geophys. Res. Lett.*, 44, 6868–6875, 2017.
- Turner, J., C. Holmes, T. Caton Harrison, T. Phillips, B. Jena, T. Reeves-Francois, R. Fogt, E. R. Thomas, and C. C. Bajish: Record low Antarctic sea ice cover in February 2022. *Geophys. Res. Lett.*, 49, e2022GL098904, 2022.
- Windnagel, A., Meier, W., Stewart, S., Fetterer, F., & Stafford, T.: NOAA/NSIDC Climate Data Record of Passive Microwave Sea Ice Concentration Version 4 Analysis. NSIDC Special Report 20. Boulder CO, USA: National Snow and Ice Data Center, 2021.
- World Meteorological Organization: WMO sea-ice nomenclature. Terminology, codes and illustrated glossary. Geneva, Secretariat of the World Meteorological Organization, 1970. [ix], 147 p. [including 175 photos] + corrigenda slip. (WMO/OMM/BMO, No. 259, TP. 145.). Edition 1970.
- Zygmuntowska, M., P. Rampal, N. Ivanova, and L. H. Smedsrud: Uncertainties in Arctic sea ice thickness and volume: new estimates and implications for trends, *The Cryosphere*, 8 (2), 705–720, doi:10.5194/tc-8-705-2014, 2014.